

Mineral equilibria at high PT-parameters

**Butvina V.G.¹, Safonov O.G.^{1,2}, Spivak A.V.¹,
Limanov E.V.¹, Vorobey S.S.³, Bondarenko
G.V.¹, Van K.V.¹ Synthesis of k-ba titanates of
the magnetoplumbite group at high pressure.
UDC: 552.13**

¹ Institute of Experimental Mineralogy RAS, Chernogolovka

² Lomonosov Moscow State University, Moscow

³ Vernadsky Institute of Geochemistry and Analytical
Chemistry of the Russian Academy of Sciences, Moscow
butvina@iem.ac.ru

Abstract. Paper presents the results of an experimental study on the crystallization of Cr-bearing K-Ba-titanates of the magnetoplumbite group (yymengite and hawthorneite) in the chromite-rutile/ilmenite system in the presence of H₂O-CO₂-KCO₃/BaCO₃ fluid at pressures of 3.5 and 5.0 GPa and a temperature of 1200 °C, simulating the formation of these phases during metasomatism of the upper mantle peridotites. The experiments were carried out using two types of the anvil-with-hole high-pressure devices (IEM RAS), i.e. NL-40 (3.5 GPa, 1200°C) and toroidal NL-13T (5.0 GPa, 1200°C). The experiment showed that yymengite and hawthorneite were formed in the entire studied pressure range. In a system with ilmenite, minerals of the magnetoplumbite group are preferably crystallized in comparison to titanates of the hollandite group. Raman spectra of yymengite and hawthorneite are presented. The structure of the yymengite is refined.

Keywords: modal mantle metasomatism, magnetoplumbite group, hawthorneite-yymengite solid solution (HAYI), high-pressure experiment, aqueous-salt fluid

The type of mantle metasomatism expressed in the formation of new phases uncharacteristic for peridotites and eclogites is called "modal or explicit mantle metasomatism" according to the proposal of B. Harte (Harte, 1983). This process is expressed in the formation of amphiboles, phlogopite, apatite, carbonates, sulfides, titanite, ilmenite, rutile. During this process, unique mineral phases also appear, occurring only in the products of metasomatism in the mantle. Among them, the minerals of the groups of magnetoplumbite (hawthorneite-yymengite), crichtonite (lindsleyite-mathiasite) and hollandite (redledgeite-pryderite) (Haggerty, 1991) are particularly distinguished - rare K-Ba titanates enriched with large-ionic lithophilic (LILE), highly charged (HFSE), light rare-earth (LREE) elements, as well as U and Th.

Yimengite K(Cr, Ti, Mg, Fe, Al)₁₂O₁₉ is the mineral of magnetoplumbite group PbFe₁₂O₁₉ (example, Haggerty, 1991) with formulae AM₁₂O₁₉. Position A with coordination 12 in the structure of the barium ferrite type (BaFe₁₂O₁₉) of this mineral is located in perovskite-like layers (AMO₃) and contains large cations (K, Ba and other LILE), while

small cations M (Ti, Cr, Fe, Mg, Zr, Nb, V, Zn) are located in polyhedra with coordination 4 and 6 in spinel-like layers (Gray et al., 1987). Yimengite forms a limited solid solution with hawthorneite Ba(Cr, Ti, Mg, Fe, Al)₁₂O₁₉ (Haggerty et al., 1989). Natural minerals of the yimengite-hawthorneite series usually do not correspond to the ideal formula, characterized by significant variations in the content of components in both positions and the presence of vacancies in the structure. Yimengite was first described in kimberlite dikes of Shandong Province, China (Dong et al., 1983) in association with olivine, pyrope, chromite, phlogopite, ilmenite, chromium diopside, apatite, zircon, moissanite. As a product of changes in chromite xenocrystals, yimengite was detected in a heavy concentrate from kimberlite sill in the Guaniamo region, Venezuela (Nixon, Condliffe, 1989) and in the kimberlites of Turkey Well, Australia (Kiviets et al., 1998). In all cases, yimengite contains BaO (up to 3.4 wt. % in yimengite from Venezuela), indicating a solid solution with hawthorneite (Gray et al., 1987; Haggerty et al., 1989; Peng, Lu, 1985). The compositional characteristics of chromites, according to which yimengite develops, indicate that they belong to the associations of diamond-bearing garnet harzburgites (Nixon, Condliffe, 1989). Yimengite inclusions have been found in diamonds (Sobolev et al., 1988, 1998; Bulanova et al., 2004), where it is also associated with typomorphic minerals of the harzburgite association: chromite, subcalcium chromium garnet, enstatite.

Yimengite inclusions described in the work of G. P. Bulanova et al. (Bulanova et al., 2004) contain elevated concentrations of Rb, Cs, Sr. So, according to some authors, yimengite is the product of reactions of diamond-bearing harzburgites composing the base of the lithospheric continental mantle at depths of about 150 km, with fluids enriched with K, HFSE, LREE. This is confirmed by the discovery of yimengite and hawthorneite in a metasomatic vein cutting harzburgite xenolith from kimberlites of the Bullfontein tube (South Africa), together with phlogopite, potassium richterite, minerals of the lindsleyite-mathiasite group, armalcolite, rutile, ilmenite (Haggerty et al., 1987).

This work is a logical continuation of the published series of experimental works by the author (Butvina et al., 2019, 2021, 2022; Butvina et al., 2020) on the formation of rare titanates as a result of metasomatic reactions. This paper publishes the results of an experimental study of the synthesis of K-Cr/Ba-Cr end members of a solid solution: hawthorneite-yimengite of the magnetoplumbite

group at 1.8-2.0; 3.5; 5.0 GPa, 900-1200°C. The experiments were carried out using high-pressure apparatuses (1) "cylinder-piston" CP-40 (1.8-2.0 GPa, 900-1000 °C), (2) "anvil with a hole" NL-40 (3.5 GPa, 1200 °C) and (3) "anvil with a hole" NL-13T (5 GPa, 1200 °C) in the Laboratory of Metamorphism, Magmatism and Geodynamics of the Lithosphere of the D.S. Korzhinsky Institute of Experimental Mineralogy of the Russian Academy of Sciences.

Natural chromite of the composition $(\text{Mg}_{0.49-0.54}\text{Fe}_{0.50-0.54}\text{Mn}_{0.01-0.02}\text{Zn}_{0.01-0.02})(\text{Al}_{0.17-0.20}\text{Cr}_{1.55-1.61}\text{Fe}_{0.10-0.22}\text{Ti}_{0.03-0.07})\text{O}_4$ from garnet lherzolite xenolith from the Pionerskaya kimberlite pipe (Arkhangelsk region), ilmenite of the composition $\text{Fe}_{0.98}\text{Mg}_{0.01}\text{Mn}_{0.06}\text{Ti}_{0.93}\text{Al}_{0.01}\text{Nb}_{0.01}\text{O}_3$, represented by a xenocrystal from kimberlite of Udachnaya tube (Yakutia), and a synthetic powder TiO_2 . The fluid component was prepared from a mixture of synthetic K_2CO_3 /or BaCO_3 and oxalic acid. The composition of the phases was determined by X-ray spectral microanalysis on a Tescan Vega-II XMU scanning electron microscope equipped with an INCA Energy 450 X-ray registration and composition calculation system in the EDS mode at an accelerating voltage of 20 kV, a current of 400 pA and an electron beam diameter of 157-180 nm (for chemical composition analysis) or 60 nm (for obtaining images). Raman spectra of titanates were obtained using a Renishaw RM1000 raman spectrometer equipped with a Leica microscope. A diode-pumped solid-state laser with a wavelength of 532 nm and a power of 20 MW was used. The spectra were recorded at 50x magnification for 100 seconds.

The chromite-ilmenite - H_2O - CO_2 - K_2CO_3 system.

In the products of experiments involving ilmenite, mathiasite is not the predominant phase, and yimengite was identified along with priderite (Fig.1a). In addition to the starting chromite and magnesian ilmenite, newly formed more ferruginous chromite and rutile were found in the products of these experiments. In experiments with different starting ratios of chromite and ilmenite, priderite and yimengite coexist. In addition to inclusions in the priderite, yimengite also forms accretions with chromite similar to accretions known in natural associations (Nixon, Condliffe, 1989). Comparison of experiments B1 and B2 shows that different starting ratios of chromite and ilmenite do not affect the phase composition of the experimental products. The structure of yimengite with the chemical formula $\text{K}_{0.90}\text{Ti}_{5.16}\text{Cr}_{2.94}\text{Fe}_{2.54}\text{Mg}_{0.87}\text{Al}_{0.22}\text{Mn}_{0.30}\text{O}_{19}$ (Fig. 2) was studied by single-crystal X-ray diffraction analysis using a synchrotron radiation source (KISI-Kurchatov) and Raman spectroscopy (RAMAN) (Butvina et al., 2023).

The chromite-ilmenite- H_2O - CO_2 - BaCO_3 system.

At 3.5 and 5 GPa, 1200°C, the following phases are formed in this system: modified chromite, ilmenite, Nb-containing rutile, hawthorneite (Fig.1b), lindsleyite. hawthorneite and lindsleyite have been identified, which form idiomorphic octahedral and subidiomorphic grains of 20-40 microns or less in size. There are individual xenomorphic grains with a size of 100 microns or more. At 1.8 GPa, 1000°C, the following phases are formed in this system: modified chromite, ilmenite, Nb-containing rutile, redledgeite, hawthorneite. Hawthorneite is found in the form of individual angular grains up to 150 microns in size, isometric shape. Redledgeite with a size of less than 30 microns forms lighter oval or isometric inclusions in altered chromite.

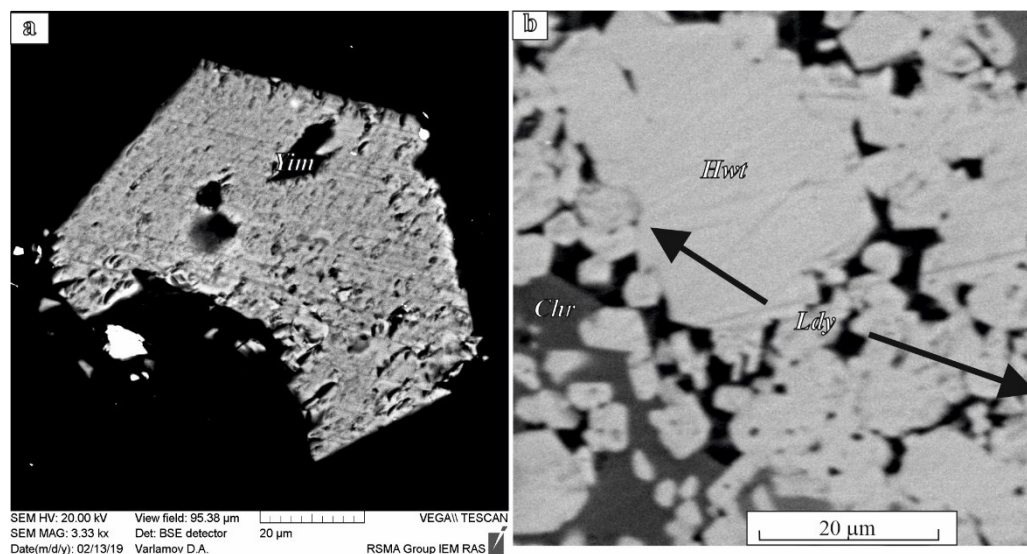


Fig. 1. SEM image in reflected electrons of synthesized yimengite (a, Yim); b hawthorneite (b, Hwt) in the chromite-ilmenite- H_2O - CO_2 - K_2CO_3 / BaCO_3 system at 5 GPa.

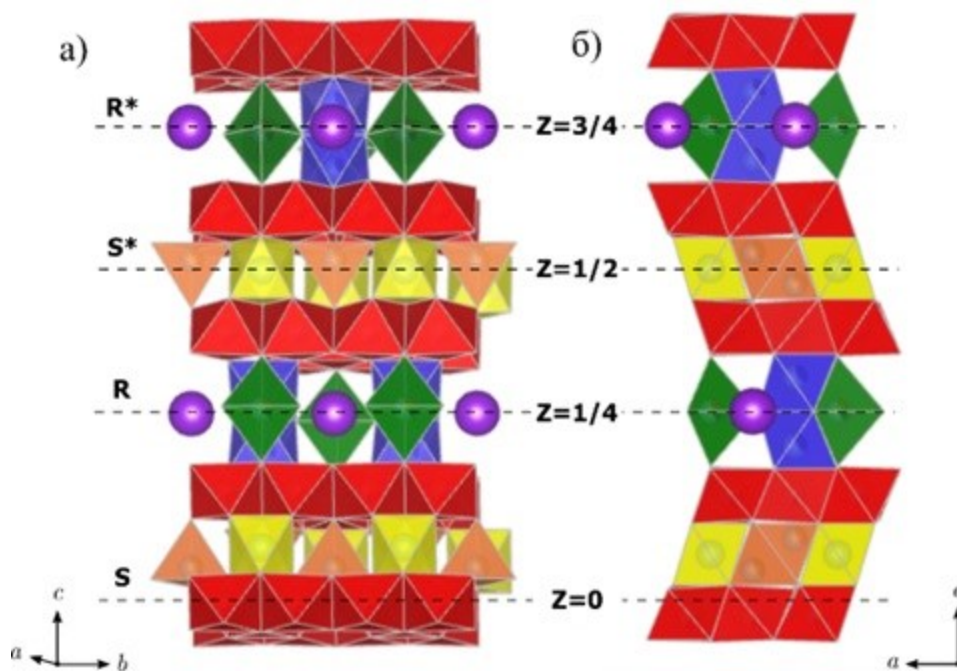


Fig. 2. The structure of the yimengite.

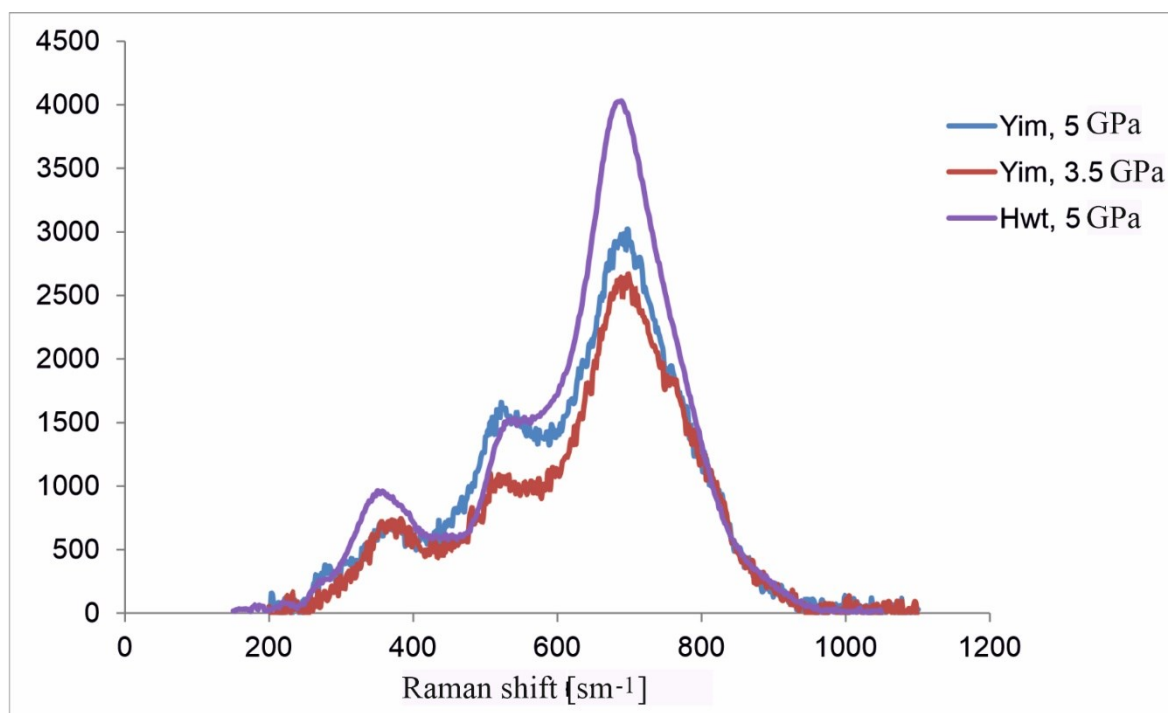


Fig. 3. Raman scattering spectra of synthesized minerals of the magnetoplumbite group (yimengites and hawthorneite).

RAMAN spectroscopy.

The presence of yimengite and hawthorneite was confirmed by RAMAN spectroscopy. The Raman spectra of yimengites were obtained in the range of 200-1200 cm^{-1} (Fig. 3). In the spectra of synthesized yimengite at 5.0 GPa, intense peaks at 357-382 (wide wave excitation region), 532, 692 and a small disturbance at 746 cm^{-1} are distinguished, in the spectra of synthesized yimengite at 3.5 GPa, intense peaks at 354-381 (wide wave excitation

region), 522, 689 and a small disturbance at 750 cm^{-1} , as can be seen, the spectra are almost identical. Intense peaks at 357, 539 and 689 cm^{-1} in the spectrum of hawthorneite (yellow band in Fig. 3) are completely comparable to the peaks in the spectra of synthetic yimengites (blue and orange bands in Fig. 3).

Thus, as a result of experimental study of the reaction of chromite and rutile, as well as chromite and ilmenite with a K water-carbonate fluid (melt),

pairs of titanate phases (priderite, yimengite and yimengite, mathiasite) were obtained – mineral indicators of mantle metasomatism, which directly confirms the possibility of the formation of yimengite, mathiasite and K–Cr-priderite, as well as other titanates, as a result of mantle metasomatism of upper mantle peridotites under conditions of the highest potassium activity (Safonov, Butvina, 2016). The experiments conducted for the first time showed the possibility of joint crystallization of Cr-containing Ba titanates as a result of the reaction of high-chromium spinel and rutile/ilmenite with Ba water-carbonate fluid (melt) in the conditions of the upper mantle. The crystallization ability of Cr-containing titanates of the magnetoplumbite group in the entire pressure range from 1.8 to 5.0 GPa has been confirmed. It is shown that minerals of the magnetoplumbite group crystallize more preferably in a system with ilmenite compared to titanates of the hollandite group. Raman scattering (RAMAN) spectra of yimengite and hawthorneite are presented. The structure of the yimengite is obtained.

The work was done on FMUF topics-2022-0001 (1021060708334-5-1.5.2;1.5.6;1.5.4) the state task of the IEM RAS for 2022-2026

References

- Bulanova G.P., Muchemwa E., Pearson D.G., Griffin B.J., Kelley S.P., Klemme S., Smith C.B. (2004) Syngenetic inclusion of yimengite in diamond from Sese kimberlite (Zimbabwe) – evidence for metasomatic conditions of growth // *Lithos* 77, 181–192.
- Butvina V.G., Vorobey S.S., Safonov O.G., Bondarenko G.V. (2020) Formation of K–Cr titanates from reactions of chromite and ilmenite/rutile with potassic aqueous-carbonic fluid: experiment at 5 GPa and applications to the mantle metasomatism. *Springer Nature* 9, 201–222.
- Dong Z., Zhou J., Lu Q., Peng Z. (1983) Yimengite, $K(Cr,Ti,Fe,Mg)_{12}O_{19}$, a new mineral from China // *Kexue Tongbao, Bull. Sci.* 15, 932–936.
- Grey I.E., Madsen I.C., Haggerty S.E. (1987) Yimengite of K–Ti metasomatic origin in kimberlitic rocks from Venezuela // *Am. Mineral.* V. 72. P.633–6.
- Haggerty S.E. (1987) Metasomatic mineral titanates in upper mantle xenoliths. In *Mantle Xenoliths* (Eds. Nixon P. H.). J. Wiley and Sons Ltd., Chichester, 671–90.
- Haggerty S.E. (1991) Oxide mineralogy of the upper mantle. (Eds. Lindsley D.H.). *Oxide Minerals: Petrologic and Magnetic Significance. Reviews in Mineralogy*, 25, 355–416.
- Haggerty S.E., Grey I.E., Madsen I.C., Criddle A.J., Stanley C.J., Erlank A.J. (1989) Hawthorneite, $Ba[Ti_3Cr_4Fe_4Mg]O_{19}$: A new meta-somatic magnetoplumbite-type mineral from the upper mantle // *Am. Mineral.* V. 74. P.668–75.
- Harte B. (1983) Mantle peridotites and processes—The kimberlite sample. (Eds. Hawkesworth C.J., Norry M.J.) In: *Continental Basalts and Mantle Xenoliths*, Shiva: Cheshire, UK, 46–91.
- Kiviets G. B., Phillips D., Shee S. R., Vercoe S. C., Barton E. S., Smith C. B., Fourie L. F. (1998) $^{40}Ar/^{39}Ar$ dating of yimengite from Turkey Well kimberlite, Australia: the oldest and the rarest. Ext. Abstr. In 7th International Kimberlite Conference, 432–434.
- Nixon P.H., Condliffe E. (1989) Yimengite of K–Ti metasomatic origin in kimberlitic rocks from Venezuela. *Min. Mag.* 53, 305–309.
- Sobolev N.V., Yefimova E.S., Channer D. M. DeR., Kaminsky F.V., Lavrentyev Yu.G., Usova L.V. (1998) Composition and Processes of Deep-Seated Zones in Continental Lithosphere. Novosibirsk, 185–186.
- Sobolev N.V., Yefimova E.S., Kaminsky F.V., Lavrentiev Y.G., Usova L.V. (1988) Titanate of complex composition and phlogopite in the diamond stability field. In: *Composition and Processes of Deep Seated Zones of Continental Lithosphere.* (Eds. Sobolev N.V.) Nauka, Novosibirsk, 185–186.
- Butvina, V.G., Vorobey, S.S., Safonov, O.G. *et al.* Experimental Study of the Formation of Chromium-Bearing Priderite and Yimengite as Products of Modal Mantle Metasomatism. *Dokl. Earth Sc.* **486**, 711–715 (2019). <https://doi.org/10.1134/S1028334X19060254>
- Butvina, V.G., Safonov, O.G., Vorobey, S.S. *et al.* Experimental Study of Reactions Forming Phlogopite and Potassic Titanates as Mineral Indicators of Metasomatism in the Upper Mantle. *Geochem. Int.* **59**, 757–777 (2021). <https://doi.org/10.1134/S0016702921080024>
- Butvina V.G., Safonov O.G., Bondarenko G.V., Shapovalov Yu.B. (2022) Experimental Study of the Formation of Ba–Cr Titanates in the Fluid-Bearing Chromite–Rutile/Ilmenite System at $T = 1000–1200^\circ C$ and $P = 1.8–5.0$ GPa // *DAS*, 504(1), pp. 22–27
- Butvina V.G., Kuzmin A.V., Spivak A.V., Safonov O.G., Lazarenko V.A., Dorovatovskiy P.V. (2023) Crystal structure of synthetic yimengite – potassium titanate // *Crystallography*. (In print)

Chertkova N.V.¹, Burova A.I.^{1,2}, Spivak A.V.¹, Zakharchenko E.S.¹, Litvin Yu.A.¹, Safonov O.G.^{1,2}, Bobrov A.V.^{1,2,3}
Experimental investigation of the ilmenite-olivine-H₂O system and conditions for inclusions capturing upon diamond growth in the upper mantle. UDC: 552.18

¹D.S. Korzhinskii Institute of Experimental Mineralogy RAS, Chernogolovka, Moscow district

²Lomonosov Moscow State University, Moscow

³Vernadsky Institute of Geochemistry and Analytical Chemistry RAS, Moscow nvchertkova@gmail.com

Abstract. Primary inclusions in diamonds serve as a unique source of information about mantle minerals and

fluids. In this work, we apply a set of experimental techniques, which combines *in situ* methods for studying samples in a diamond anvil cell apparatus and methods of high-pressure synthesis in a Bridgeman-type apparatus, to investigate mineral associations and fluid phases that are stable in the $\text{FeTiO}_3\text{-Mg}_2\text{SiO}_4\text{-H}_2\text{O}$ system in the pressure range from 4 to 8 GPa and in the temperature range from 500°C to 1250°C. Obtained experimental data can be used to model the thermobaric regime of capturing of ilmenite and olivine inclusions in the presence of hydrous fluid during diamond growth in the lithosphere.

Keywords: *ilmenite, olivine, ice VII, inclusions, diamond, phase relations, upper mantle, experiment, high pressures*

Primary inclusions are a direct source of information about the chemical and phase composition of the parental medium and the conditions of diamond growth. These inclusions formed together with diamonds and were captured by growing diamonds as paragenetic phases from the parental medium. Findings of inclusions of ices VI and VII in diamonds indicate the presence of hydrous fluids at different depths of the mantle. Ilmenite and olivine were found together with ice VII inclusions (Tschauner et al., 2018). Investigation of association of ilmenite and olivine with water became the objective of this study.

A detailed analysis of the phase relations in the $\text{FeTiO}_3\text{-Mg}_2\text{SiO}_4\text{-H}_2\text{O}$ system was carried out at temperatures from 500°C to 1250°C and pressures from 4 to 8 GPa. The range of water contents in the experiments was from 14 mol.% to 80 mol.%, the ratio of ilmenite and olivine components was from 25:75 to 75:25. Distilled water and mixtures of gel oxides FeO and TiO_2 in stoichiometric proportion FeTiO_3 for the synthesis of ilmenite and the reagent Mg_2SiO_4 for the synthesis of olivine were used as starting materials. The use of optical microscopy and Raman spectroscopy as *in situ* methods for studying samples in the diamond anvil cell with external resistive heating (Chertkova et al., 2021) made it possible to analyze the state of the fluid component

in these systems and to determine the parameters of crystallization for solid phases of H_2O . During the experiments, photo and video recording of the phase transitions, observed in the sample chamber, was carried out, and the structure of the ice phases was refined using Raman spectroscopic analysis. The pressure in the sample chamber was calculated using the position of Raman line in the spectrum of ^{13}C diamond or the R1 fluorescence line in the ruby spectrum in accordance with the calibration data (Schiferl et al., 1997; Zha et al., 2000; Ragan et al., 1992). During experiments, the temperature was measured by a PtRh–Pt thermocouple (R-type, 13% Rh, and S-type, 10% Rh were used), while its junction was fixed in the immediate vicinity of the sample. After quenching, the products of the experiments were additionally analyzed using X-ray diffraction analysis and micro-X-ray spectral (microprobe) analysis.

A series of experiments in a Bridgeman-type "anvil-with-hole" press allowed us to carry out a detailed analysis of the chemical composition for coexisting phases, which are stable in the chosen system at high temperatures. The mineral associations obtained in the experiments include (Table 1): ilmenite + olivine, ilmenite + pyroxene + humite group minerals. With the increase of olivine fraction in the starting materials, the content of pyroxene and humite group minerals increased in the run products. Ilmenite was the main titanium concentrating mineral in the experiments, at the same time, with the increase of magnesium content in the starting composition, more magnesium entered the structure of ilmenite, up to the formation of picroilmenites. The content of titanium in pyroxenes was ~2 wt.%, in minerals of the humite group its content reached 7.3 wt.%. Minerals of the humite group obtained in experiments are characterized by isomorphic substitution of the type: $3\text{Mg}^{2+}=\text{Ti}^{4+} + \text{Fe}^{2+}$.

Table 1. Conditions and results of experiments in the ilmenite-olivine-water system.

Run number	The ratio of Ilm and Ol components in the start mixture	T, °C	P, GPa	t, min	Experimental products
3285	Ilm : Ol = 75 : 25	1250	6	60	Ilm, Ol
3284	Ilm : Ol = 50 : 50	1250	6	60	Ilm, Px, Hum
3286	Ilm : Ol = 25 : 75	1250	6	60	Ilm, Px, Hum

Abbreviations: Ilm – ilmenite, Ol – olivine, Px – pyroxene, Hum – minerals of the humite group.

Experiments, carried out in the $\text{SiO}_2\text{-TiO}_2\text{-FeO-MgO-H}_2\text{O}$ system at P-T parameters of the upper mantle in the stability field of diamond, showed possible phase reactions between olivine, ilmenite and hydrous fluid with the formation of new phases - pyroxene and humite group minerals.

Comparing the assemblage of mineral phases obtained in experiments with the literature data (Tschauner et al., 2018), which describe coexistence of ice VII inclusions with ilmenite in association with olivine, one can make an assumption about the stability of such association in the system with

olivine content of 25 mol.% or less. At higher contents of the olivine component, a phase reaction with the formation of pyroxene and minerals of the humite group is expected. Since the silicate components have an inhibitory effect on the spontaneous nucleation of diamond, their content should not exceed 35 wt.% in the diamond-forming growth medium (Bobrov and Litvin, 2009), which is consistent with the data on phase relations obtained in this work. At the same time, the intergrowths of olivine and ilmenite in inclusions in Yakutian diamonds described by Sobolev et al. (1997) could have formed in a system rich in ilmenite, which emphasizes the uniqueness of this paragenesis.

The use of innovative methods of *in situ* analysis in a high-pressure diamond anvil cell with external heating in combination with traditional methods of high-pressure synthesis in this work gave an opportunity to obtain new experimental data on phase relationships and possible phase reactions in the systems, modeling the processes of growth and capturing of mineral and fluid inclusions by diamonds in the Earth's upper mantle.

Acknowledgments: This work was carried out with the support of the Russian Science Foundation (project No. 20-77-00079) and partially within the Research program FMUF-2022-0001 of the Korzhinski Institute of Experimental Mineralogy RAS

References

1. Bobrov AV, Litvin Yu. A. Peridotite-eclogite-carbonatite systems at 7.0-8.5 GPa: concentration barrier of diamond nucleation and syngensis of its silicate and carbonate inclusions // *Geology and Geophysics*. - 2009. - T. 50. - No. 12. - S. 1571-1587. (in Russian)
2. Chertkova N.V., Spivak A.V., Zakharchenko E.S., Litvin Yu.A., Safonov O.G., Novikov A.P., Efimchenko V.S., Meletov K.P. High-pressure installation with external heating for in situ studies of phase transitions // *Instruments and Experimental Technique*. - 2021. - No. 3. - S. 158-160. (in Russian)
3. Logvinova A. M., [Richard Wirth](#), [Ekaterina N. Fedorova](#), [Nikolai V. Sobolev](#). Nanometre-sized mineral and fluid inclusions in cloudy Siberian diamonds: new insights on diamond formation // *European Journal of Mineralogy*. - 2008. - V. 20. - No. 3. - C. 317-331.
4. Logvinova A.M., [R. Wirth](#), [A.A. Tomilenko](#), [V.P. Afanas'ev](#), [N.V. Sobolev](#). The phase composition of crystal-fluid nanoinclusions in alluvial diamonds in the northeastern Siberian Platform // *Russian Geology and Geophysics*. - 2011. - T. 52. - No. 11. - C. 1286-1297.
5. Ragan D.D., Gustavsen R., Schiferl D. [Calibration of the ruby R1 and R2 fluorescence shifts as a function of temperature from 0 to 600 K](#) // *J. Appl. Phys.* - 1992. - V. 72. - No. 12. - P. 5539.
6. Schiferl, David & Nicol, Malcolm & Zaug, Joseph & Sharma, Shiv & Cooney, T. & Wang, SY & Anthony, Thomas & Fleischer, James. The diamond ¹³C/¹²C isotope Raman pressure sensor system for high-temperature/pressure diamond-anvil cells with reactive samples // *Journal of Applied Physics*. - 1997. - 82. - P. 3256 - 3265.
7. Sobolev N.V., Kaminsky F.V., Griffin W.L., Yefimova E.S., Win T.T., Ryan C.G., Botkunov A.I. Mineral inclusions in diamonds from the Sputnik kimberlite pipe, Yakutia // *Lithos*. - 1997. - T. 39. - No. 3-4. - C. 135-157.
8. Tschauner O., S. Huang, E. Greenberg, V. B. Prakapenka, C. Ma, G. R. Rossman, A. H. Shen, D. Zhang, M. Newville, A. Lanzirotti, K. Tait. Ice-VII inclusions in diamonds: Evidence for aqueous fluid in Earth's deep mantle // *Science*. - 2018. - V. 359. - No. 6380. - C. 1136-1139.
9. Zha C.S., Mao H.K., Hemley R.J. Elasticity of MgO and a primary pressure scale to 55 GPa // *Proceed. Nat. Acad. Sci.* - 2000. - V. 97. - 25. - C. 13494-13499.

Fedkin V.V. Origin of contrast series of rocks in the crust eclogite-blueschist complexes.
UDC: 549.6+552.16:552.48

D.S. Korzhinskii Institute of Experimental Mineralogy (IEM RAS) vfedkin@iem.ac.ru

Abstract. The eclogite-blueschist complexes usually contain contrasting series of rocks characterized by a high degree of their alteration (metamorphism). These are eclogite bodies, blocks, boudins, interlayers and lenses included in the metasedimentary or granitoid thickness of the host rocks, which are not having of clear high pressure (HP) characteristics of their origin. The mineralogical thermobarometry method was used to carry out a detailed analysis of the P-T conditions of formation contrasting series of rock for the Atbashi eclogite-blueschist complex (Southern Tien Shan). High-pressure rocks, eclogite boudins, and bodies in contact with host metasedimentary strata were formed in the process of tectonic melange at an early stage of the development of the complex - the model of tectonic melange (TM-model). The enclosing gneiss-schist matrix with the participation of Grt-Cpx gneisses, Grt-Cpx-Gln, micaceous and chlorite schists, diaphthorites, quartzites and quartzite schists were formed as a result of coherent development of complex at a later regressive stage of metamorphism - the model of coherent formation of layered strata (CU- model). As a result, for the Atbashi complex a low geothermal gradient (~ 10 deg/km) was recorded at the initial stage of its development with maximum parameters up to $t = 650-700$ °C and $P = 14-15$ kbar (for Grt-Cpx rocks and eclogites). Intermediate stage of metamorphic evolution has characterized by change in direction of P-T trend of metamorphic conditions as "clockwise", which is characterized of intracontinental sutures. The minimum parameters in the form of a regressive P-T trend show the level of metamorphic conditions of the green-schist-blueschist facies in the temperature range from 250-300 to 500-550 °C and pressures from 2-4 to 8-10 kbar.

Keywords: HP-UHP metamorphic rocks, formation conditions of contrasting series of rocks, Atbashi eclogite-

blueschist complex, tectonic mélange, coherent development, P-T trend of metamorphic evolution.

High-pressure (HP) eclogite-glaucophane schist/blueschist complexes, as a rule, form in the junction zones of large geosubstructural elements of the Earth's crust under conditions of constant tectonic activity and changing metamorphism regime (Dobretsov and Sobolev, 1977, Dobretsov et al., 1996). Due to these circumstances, blocks of basic rocks metamorphosed at high and ultrahigh pressures (HP-UHP) are often included as separate bodies, boudins, interlayers and lenses in metasedimentary or granitoid rocks. In the Atbashi eclogite-blueschist complex, the mixed composition of host rocks - pelitic, pelitic-feldspar, mafic, quartz-carbonate rocks, quartzites and quartzite schists, does not have clear signs of HP/UHP metamorphism (Kotova, 1989; Hegner et al., 2010). The maximum pressure of their formation does not exceed 5-7 kbar, while eclogite and eclogite-like (Grt-Cpx, Grt-Cpx-Gln) mineral associations indicate higher P-T parameters: P up to 14-15 kbar (sometimes up to 17-19 kbar) in the temperature range of 350-700 °C.

The reasons for the contrasting conditions of metamorphism of eclogite boudins, blocks, and the host rock complex have not yet been fully elucidated and cause active discussion. There are two points of view to explain this phenomenon: the model of coherent formation of layered strata - CU-model (Hacker et al., 2010, Liu et al., 2001) and the model of tectonic mélange - TM-model (Meyer et al., 2014). For the Atbashi eclogite-blueschist complex, both models of the formation of contrast structures are considered, but remain controversial (Kotova, 1989, Lú, Bucher, 2018). Methods of mineralogical thermobarometry make it possible to assess the significance of these concepts in the formation of coexisting complexes of contrasting rocks.

The Atbashi eclogite-blueschist complex is part of the system of the intracontinental Ural-Tianshan Hercynian folded belt. It adjoins the HP-UHP metaophiolite belt "Chinese Western Tien Shan" and is confined to the most important tectonic boundary between the northern and southern Tien Shan - the Kansk-Atbashi deep fault. Detailed petrographic studies of eclogite-glaucophane and other associated rocks included in the Cheloktorskaya suite show that these rocks were formed under conditions of moderate pressure (up to 10-12 kbar) in the temperature range of 300-600 °C (Бакиров, 1978; Dobretsov, Sobolev, 1977; Simonov et al., 2008). Progressive processes of metamorphism and retrograde transformation of rocks (glaucophane growth, muscovitization, carbonization, etc.) proceed against the background of intense alkaline metasomatism and acid leaching. The age of

metamorphism of eclogite-glaucophane rocks of the complex is determined as 320-360 Ma (Dobretsov et al., 1996), although there are also older dates - 520-550 and even 1100 Ma. The successive transition from eclogites to Grt-Gln rocks, quartzite schists, and chlorite diaphorites builds a typical for areas of intracontinental suture structures trend of change in P-T conditions of metamorphism of the "clockwise" type with a low (~10 deg/km) geothermal gradient at the initial stage of development and maximum parameters up to T=650-700°C at P=14-15 (sometimes up to 17-19) kbar (Fedkin, 2004). The minimum P-T conditions of mineral formation in the rocks of the Atbashi complex are fixed at the level of the lower green-schist facies in the form of regressive P-T trends from T=550-570°C and P=3-5 kbar to T=350-400°C at P=0.5-2 .0 kbar. The prograde orientation of metamorphic processes is fixed in the progressive zoning of the main rock-forming minerals - garnet, clinopyroxene, and plagioclase. Retrograde transformation of rocks took place against the background of intense acid leaching and magnesian metasomatism.

The methods of mineralogical thermobarometry were used, to study the conditions for the formation of contrasting series of high-pressure and host rocks, which make it possible to assess the significance of one or another mechanism for the formation of these series for a particular complex (Korikovskii, 1995). The problem is solved on the basis of data on the Grt-Cpx-Pl-Qtz equilibrium, the main information source of the conditions for the formation of HP rocks in eclogite-blueschist complexes. Samples of different contrasts from eclogite and host rocks were studied by microprobe. The composition and zoning of the main rock-forming and accompanying minerals, their contacts, mineral inclusions, and reaction relationships are analyzed. The data obtained made it possible to determine the P-T parameters of the formation of mineral associations, the direction (P-T trends) and features of the evolution of metamorphism at different stages of the development of the complex. The Grt-Cpx geothermometer (Powell, 1985) and the Ab-Jd-Qtz geobarometer (Perchuk, 1992), as well as other mineralogical tools used in petrology, were used to estimate the parameters of mineral formation and plot P-T trends.

Mass determinations of the formation parameters of Grt-Cpx associations of representative samples of contrasting series of rocks of the complex demonstrate a principal different evolutionary history of their formation. In the central areas of large eclogite boudins and individual isolated bodies, the progressive zoning of garnet (XPrp=0.11-0.53) and the omphacite composition of pyroxene (XJd=0.4-0.6) fix prograde P-T metamorphism trends with low

(~10 deg /km) geothermal gradient and parameters up to T=650-700 °C and P=14-15 kbar, sometimes up to 18-19 kbar. (Fig. 1a).

These conditions, most likely, arose at an early stage of the formation of the complex and were preserved in the bodies of eclogites as a result of tectonic mélangé. The rocks in contact with them - Grt-Am gneisses and shales have preserved traces of prograde metamorphism of boudins, developing an eclogitic P-T trend to low temperatures down to T=300-550 °C at P=8-10 kbar (Fig. 1a). As we move away from the central part of the boudina, in the marginal parts of the eclogitic bodies and in their immediate surroundings, prograde changes in the composition of coexisting phases cover an ever wider

range of compositions of eclogites and surrounding rocks, in which sufficiently high parameters and a progressive direction of Grt-Cpx and Grt are still preserved. -Am trending. At the same time, negative P-T trends are already appearing in the low-pressure Grt-Chl matrix associations (Fig. 1b).

The coherent stage of development of the complex is characterized by a noticeable decrease in pressure in the Grt-Am paragenesis to 5-6 kbar at T=550-600 °C and a significant reversal of P-T trend clockwise - “clockwise” (Fig. 2). Prograde P-T trends in the Grt-Gln-Chl schist sequence change to retrograde ones, eclogites and Grt-Cpx associations disappear from the section, and multidirectional zoning of minerals is formed.

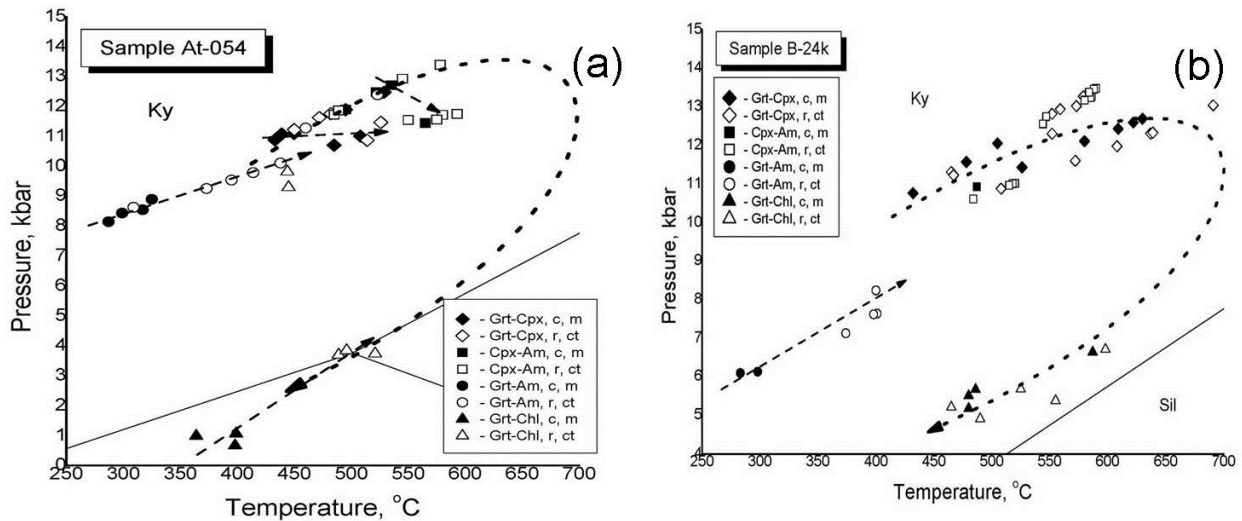


Fig. 1. P-T conditions of formation of high-pressure (HP) rocks of the Atbashi eclogite-blueschist complex, preserved as a result/process of tectonic mélangé: (a) prograde P-T trend in eclogite from the central part of the boudina; (b) conjugated prograde P-T trends in Grt-Cpx and Grt-Am associations from Grt-Cpx-Am gneiss at contact with eclogite in the host Grt-Gln-Chl schist.

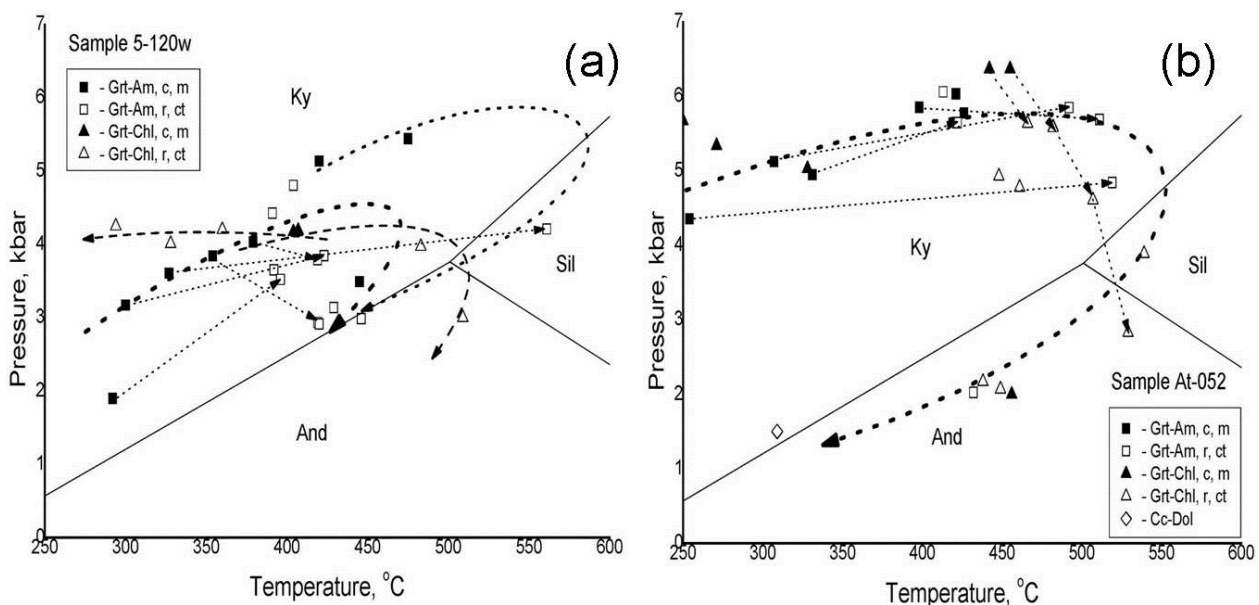


Fig. 2. Coherent stage of development of the Atbashi eclogite-blueschist complex: (a) change in the direction of P-T metamorphism trends clockwise in the Grt-Am and Grt-Chl parageneses; (b) the final stage of the coherent formation of the Atbashi complex under the conditions of retrograde low-pressure metamorphism.

The progressive zoning of the main eclogitic minerals (Grt, Cpx, etc.) reverses, marking the beginning of the retrograde stage of metamorphism. In the Grt-Cpx and Grt-Cpx-Gln crystalline schists of the matrix complex, second-generation pyroxene with a minimum proportion of the jadeite component ($X_{Jd}=0.03-0.08$) is formed. This composition of Cpx in equilibria with garnet from the matrix rocks shows parameters fundamentally different from P-T conditions for the eclogite boudins formation. A wide range of compositions of rocks of the gneissic stratum forms series of differently directed P-T trends, characterizing the conditions of their joint, coherent origin.

In low-temperature chlorite schist and diaphthorites of the host complex the retrograde P-T metamorphic trends are recorded in Grt-Chl associations in the range from $P=4.0-3.5$ kbar and $T=550-500$ °C, to $P=2.0-1.2$ kbar and $T=450 - 300$ °C, which refer to the final stage of its coherent development.

Conclusion. Methods of mineralogical thermobarometry and data on the Atbashi eclogite-blueschist complex confirm the idea of the formation of contrasting rocks in crustal eclogites (**Korikovskiy, 1995**) as a result of tectonic melange at an early stage of the development of the complex (eclogitic bodies, blocks, boudins) and coherent processes of the host rocks formation at regressive stage of its development.

The conditions for the formation of contrasting series of the Atbashi complex fundamentally differ from each other.

- The metamorphism rank for the initial stage of formation of the complex - for blocks and inclusions of HP rocks - is an order of magnitude higher than for the enclosing gneiss-shale complex. This level reaches the values of $T=650-700$ °C and P up to $P=13-19$ kbar and $T=300-550$ °C at $P=1.2-6.0$ kbar, respectively;
- High-pressure rocks of boudins and blocks are characterized by prograde direction of evolution of P-T parameters of metamorphism. For the host complex of rocks it is, retrograde, and there is a characteristic clockwise P-T trend reversal in the transition zone, ;
- Rock-forming minerals in eclogite bodies and boudins shows the maximum values of the main composition parameters: X_{Prp} in Grt up to 0.40-0.53, X_{Jd} in Cpx up to 0.50-0.66, X_{An} in Pl up to 0.20-0, 40 and the prograde zoning of phases from the center to the edge of the grain;
- The rocks of the host complex are characterized by inversion zoning of

coexisting phases with a wide range of compositions in the transitional area and regressive zoning with minimal values of composition parameters for retrograde rocks and diaphthorites;

- The coherent stage of the formation of the host complex is characterized by active manifestations of metasomatic processes: albitization of plagioclase, carbonization of Cpx associations, general silicification of rocks, manifested at the regressive stage of metamorphism and diaphthoresis.

However, the significance of these differences should not be overestimated, since in the course of development of the complex they are erased and become less noticeable and effective due to the subsequent metamorphic events.

Acknowledgements

The author is grateful to the staff of the M.M. Adyshev Institute of Geology of the National Academy of Sciences of the Kyrgyz Republic for the opportunity to conduct joint field work on the Atbashi eclogite glaucophane-schist complex, for creative and useful discussion of the results.

Funding sources: state order FMUF-2022-0004, reg. No. 1021051302305-5-1.5.2; 1.5.4, RFBR grant 05-05-64561, and the Fulbright Program of the Institute of International Education, grants 2011 and 2015.

References

- Bakirov A. 1978 Tectonic position of the Tien Shan metamorphic complexes. // "Ilim". Frunze. 262 p.
- Dobretsov N.L., Sobolev N.V. 1977. Glaucophane-schist belts. // In the book. Metamorphic complexes of Asia. N: Science, pp.283-288.
- Dobretsov N. L., Shatsky V. S., Coleman R. G., Lennykh V. I., Valizer P. M., Liou J. G., Zhang R. and Beane R. J. 1996. // International Geology Review, v. 38, p. 136-160.
- Fedkin V.V. 2004. Mineralogical geothermobarometry in developing metamorphic systems. // On Sat. "Experimental mineralogy: some results at the turn of the century". M. Science, vol. 2, pp. 172-187.
- Hacker, B.R., Andersen, T.B., Johnston, S., Kylander-Clark, A.R.C., Peterman, E.M., Walsh, E.O., Young, D., 2010. High-temperature deformation during continental-margin subduction & exhumation: the ultrahigh-pressure Western Gneiss Region of Norway // Tectonophysics 480. 149-171.
- Hegner, E., Klemd, R., Kroner, A., Corsini, M., Alexeiev, D.V., Iaccheri, L.M., Zack, T., Dulski, P., Xia, X., Windley, B.F., 2010. Mineral ages and P-T conditions of late Paleozoic highpressure eclogite

- and provenance of M Lange sediments from Atbashi in the South Tianshan Orogen of Kyrgyzstan. *Am. J. Sci.* 310, 916–950.
- Korikovsky S.P. 1995 Contrasting models of prograde-retrograde metamorphism evolution of Phanerozoic fold belts in collision and subduction zones. // *Petrology*. T.3. No. 1. pp. 45–63.
- Kotova L.S. 1989. Petrochemical evolution of the eclogite-glaucophane schist complex of the Atbashi Ridge (Southern Tien Shan). // *On Sat. Geochemistry of igneous and metamorphic formations of the Tien Shan*. Fr.: Ilim, p. 110–127.
- Liu, F., Xu, Z., Yang, J., Maruyama, S., Liou, J.G., Katayama, I., Masago, H., 2001. Mineral inclusions of zircon and UHP metamorphic evidence from paragenesis and orthogneiss of pre-pilot drillhole CCSD-PP2 in north Jiangsu Province, China. // *Chin. Sci. Bull.* 46, 1038–1042.
- Lü Z., Bucher K. 2018. The coherent ultrahigh-pressure terrane of the Tianshan meta-ophiolite belt, NW China. // *Lithos* 314–315. 260–273.
- Meyer, M., Klemd, R., Hegner, E., Konopelko, D., 2014. Subduction and exhumation mechanisms of ultrahigh and high-pressure oceanic and continental crust at Makbal (Tianshan, Kazakhstan and Kyrgyzstan). // *J. Metamorph. Geol.* 32, 861–884.
- Perchuk, A.L., 1992. New variant of the omphacite–albite–quartz geobarometer taking into account the structural states of omphacite and albite. *Dokl. Akad. Nauk* 324(6), 1286–1189.
- Powell R 1985. Regression diagnostics and robust regression in geothermometer/ geobarometer calibration: the garnet-clinopyroxene Geothermometer revisited. // *J. Metamorph. Geol.* 3, 231–243.
- Simonov, V.A., Sakiev, K.S., Volkova, N.I., Stupakov, S.I., Travin, A.V., 2008. Conditions of formation of the Atbashi Ridge eclogites (South Tien Shan). *Russ. Geol. Geophys.* 49, 803–815.

Gorbachev N.S., Kostyuk A.V., Nekrasov A.N., Gorbachev P.N., Sultanov D.M. Melting and phase relations in the basalt-FeS-Fe-C system at P= 4 GPa, T= 1400°C: Re behavior at FeS-FeC liquation of a Fe-S-C melt. UDC: 550.4.02

Korzhinskii Institute of Experimental Mineralogy RAS. e-mail: gor@iem.ac.ru, nastya@iem.ac.ru

Abstract. During partial melting of the graphite-saturated Fe–S–C system with the addition of trace elements at P = 4 GPa, T=1400°C, the liquid phases are represented by immiscible Fe–S (Ms) and Fe–C (Mc) melts, which give Fe-sulfide matrix with inclusions of Fe-C globules coexisting with relics of the original Re and multiphase microcrystalline restite. Re is predominantly concentrated in the mc melt, with DMc/Ms ~ 10. At a Re concentration of Mc > 11 wt.%, saturation of the Mc melt of Re is observed with precipitation of the Fe-Re phase containing up to 25 wt.% Re. The relics of the original rhenium in the Ms melt of Fe-Re composition coexist with the Fe phase

formed as a result of the reduction of Fe²⁺ Ms by rhenium during the red-ox reaction according to the scheme: FeS (Ms) + Re = Fe + ReS (Ms) or ²⁺Fe (Ms) + 2e = ⁰Fe (Mc), ⁰Re (Mc) – 2e = ²⁺Re (Ms). Fractionation of Re relative to Os is observed when distributed between Mc-Ms melts with distribution coefficients Kd Re/Os (Mc-Ms) ~ 9. This effect will lead to a shift in the Re/Os ratio and the Re-Os system of isotopes based on the β-decay of ¹⁸⁷Re up to ¹⁸⁷Os in environments with Mc-Ms layering.

Keywords: metal, sulfide, silicate, liquation, experiment, distribution of Re

Melting and phase relationships in the basalt–FeS–Fe–C system are of interest in connection with the problems of early differentiation of cosmic bodies, the phase composition of meteorites, as well as magmatic iron–sulfide deposits, since in the presence of carbon the sulfide melt separates into Fe – metallic (Mc) and Fe–sulfide (Ms) melts, immiscible with silicate ones. Previously, based on models of homogeneous accretion of the Earth and impact melting of its matter, the early differentiation of the Earth’s matter with the formation of the Fe core and silicate mantle was associated with the separation of metallic iron melts from the silicate melt (Sorokhtin, Ushakov, 1991; Halliday, Wood, 2009). However, it turned out that during the separation of the metal component during the formation of the core, the content of high-siderophile elements (HSE) in the mantle is significantly higher than it should be, based on the equilibrium of the silicate melt with the Fe-metal during its separation (Li, Agee, 1996).

Meanwhile, based on the chondrite composition of the primary matter of cosmic bodies, similar in composition to carbonaceous chondrites, containing up to 15 wt.% Fe-FeS (Mc Donoug, Sun, 1995), the triple Fe-S-C system with immiscibility between Mc and Ms melts.

Phase relationships and distribution of trace elements in the Fe-S-C system are also of interest in connection with the problems of the genesis of magmatic sulfide deposits in the Norilsk region. The possibility of the existence of FeC-FeS liquation during their formation follows from the peculiarities of the geological setting (Gorbachev et al., 2021). When emplaced, the hypabyssal ore-bearing intrusions of the Norilsk region broke through a thick, up to 15 km, platform cover, many of whose rocks are enriched not only in sulfur, but also in carbon (carbonaceous matter, oil and gas bearing horizons). If assimilation by melts of ore-bearing intrusions of sulfur from the rocks of the platform cover is possible, which is confirmed by the isotope composition of sulfur in sulfides (δS³⁴ + 8–12‰), then carbon assimilation is quite possible, and as a result, FeC-FeS segregation of sulfide melt during carbon contamination.

The paper considers some features of the phase relationships and behavior of rhenium, osmium and platinum in the basalt-FeS-Fe-C system at 4 GPa, 1400°C.

The experiments were carried out at the IEM RAS on an anvil-and-hole setup according to the multiampoule quenching technique (Gorbachev, 1990). The temperature was measured with a Pt30Rh/Pt6/Rh thermocouple, and the pressure at high temperatures was calibrated using the quartz-coesite equilibrium. The accuracy of temperature and pressure determination is estimated at $\pm 10^\circ\text{C}$ and ± 1 kbar (Litvin, 1991). The initial sample consisted of silicate (glass of magnesian basalt) and ore (pyrrhotite - 58 wt.%, Fe - 36 wt.%, carbon black - 6

wt.%) fractions in a ratio of 1:2 with the addition of metallic Re, Os and Pt.

The quenched sample consisted of silicate and ore parts. The silicate part consists of products of partial melting of magnesian basalt, represented by restite Grt-Cpx composition and silicate glass of ferrobasalt composition in the form of intergranular melts between Grt and Cpx and massive precipitates among sulfides during the injection of silicate melt. Garnet $\text{alm}_{60}\text{-pyr}_{20}\text{-gros}_{20}$ composition $X_{\text{Mg}} = 0.42$, $X_{\text{Ca}} = 0.23$, contains ≤ 1 wt % TiO_2 and Cr_2O_3 . Clinopyroxene of diopside-hedenbergite composition $(\text{Ca}_{0.6}\text{Mg}_{0.5}\text{Fe}_{0.4})(\text{Al}_{0.3}\text{Na}_{0.1})\text{Si}_2\text{O}_6$ coexists with a silicate melt of ferrobasalt composition.

Table 1. Compositions of coexisting sulfide phases in the ore part of the sample

Phase	S	Fe	Ni	Co	Re	Os	Pt
Microcrystalline restite matrix							
1	27.04 \pm 1.04	71.67 \pm 1.22	0.43 \pm 0.14	0.77 \pm 0.11	-	0.77 \pm 0.41	0.67 \pm 0.38
2	33.97 \pm 2.75	62.51 \pm 3.03	0.22 \pm 0.12	-	-	-	-
3	-	88.01 \pm 1.61	-	-	8.88 \pm 1.49	-	-
4	-	32.57 \pm 4.59	0.13 \pm 0.06	-	65.92 \pm 4.69	1.80 \pm 0.37	-
5	-	86.19 \pm 1.35	0.39 \pm 0.25	-	11.58 \pm 2.26	-	-
Massive sulfides							
6	26.68 \pm 0.56	72.18 \pm 0.80	0.40 \pm 0.12	0.80 \pm 0.18	0.79 \pm 0.45	0.36 \pm 0.06	0.63 \pm 0.10
7	10.80 \pm 3.69	88.34 \pm 3.38	0.49 \pm 0.08	-	0.47 \pm 0.21	≤ 0.17	0.17 \pm 0.04
8	1.45 \pm 0.49	88.18 \pm 1.69	0.37 \pm 0.15	1.28 \pm 0.16	9.96 \pm 1.49	0.54 \pm 0.16	0.39 \pm 0.22
9	0.89 \pm 0.08	84.74 \pm 1.44	0.47 \pm 0.12	-	11.60 \pm 1.48	1.92 \pm 0.54	0.65 \pm 0.10
10	0.10 \pm 0.06	71.69 \pm 0.83	0.29 \pm 0.13	-	27.25 \pm 0.76	0.96 \pm 0.35	≤ 0.10
11	1.01 0.63	90.34 \pm 1.20	0.39 \pm 0.08	-	8.01 \pm 1.20	0.31 \pm 0.07	≤ 0.10
Rhenium relics in massive sulfides							
12	-	32.57 \pm 4.59	0.13 \pm 0.06	-	65.92 \pm 4.69	1.80 \pm 0.37	-
13	1.42 \pm 0.85	88.73 \pm 1.69	0.36 \pm 0.20	-	8.86 \pm 1.99	-	-

Note: Microcrystalline restite matrix: 1 – bulk composition; 2 - sulfides; 3 – Fe-metal phase; 4 - relics of rhenium; 5 – Fe-metal phase at contact with rhenium relics. Massive sulfides: 6 – bulk composition; 7 – quenching metal phase; 8 – bulk composition of Fe-metal globules without inclusions; 9 – bulk composition of Fe-metal globules with rhenium phase inclusions; 10 – rhenium phase inclusions in Fe-metal globules; 11 – matrix of Fe-metal globules with rhenium phase inclusions. Rhenium relics in massive sulfides: 12 – rhenium relics; 13 – Fe-metal phase at contact with rhenium relics.

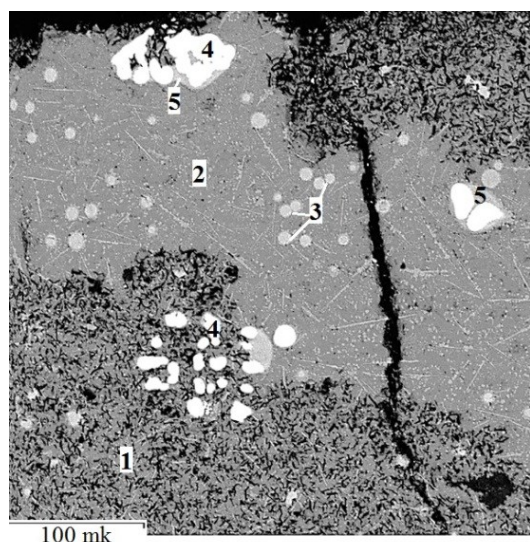


Fig. 1. BSE micrograph of the ore part of the quenched sample, characterizing the phase relationships: 1) microcrystalline matrix, 2) massive sulfides, 3) Fe-metal globules, 4) rhenium relics, 5) Fe-Re phase at contact with rhenium relics.

The "mineral chaos" of the microcrystalline matrix consists of a mixture of micron-sized particles of a sulfide, metallic composition, with inclusions of relics of rhenium in association with the Fe-metal phase. Bulk composition: Fe - 72 wt.% and S - 27 wt.%, content of Ni, Co, Re, Os, Pt 0.4–0.8 wt.%.

The matrix of massive sulfides contains inclusions of globules of the Fe-metal phase, single-phase, without inclusions and polyphase, with

inclusions of the Fe-Re phase, as well as relics of rhenium in contact with the Fe-metal phase. Its composition, taking into account the hardening phases, corresponding to the composition of the sulfide melt, is characterized by an excess sulfur content relative to troilite, low (0.4–0.8 wt.%) contents of each of the ore elements Ni, Co, Re, Os, Pt.

Table 2. Compositions of Mc and Ms melts, ratios and distribution coefficients of Re/Os and Pt/Os between them.

	Mc	Ms	D ^{Mc/Ms}
Fe	88,18	72,18	1,22
Ni	0,37	0,4	0,92
Re	9,96	0,79	12,64
Os	0,54	0,36	1,51
Pt	0,39	0,63	0,62
S	1,45	26,68	0,05
Co	1,28	0,80	1,60
Re/Os	18,44	2,2	8,37 (Kd)
Pt/Os	0,72	1,77	0,41 (Kd)

Fe-metal globules are the products of quenching of the Fe-metal melt (Mc), immiscible with the sulfide (Ms) melt, formed during separation (liquation) of the C-containing sulfide melt.

Single-phase Fe-metal globules, corresponding to the composition of the Fe-metal melt coexisting with the sulfide melt, are characterized by high contents of Fe (87–89 wt.%), Re (8–11 wt.%), contain up to 1.3 wt.% Co, about 0.3–0.6 wt.% Ni, Os, Pt.

Polyphase, rhenium-saturated Fe-metal globules, with inclusions of the Fe-Re phase, composition 72 wt.% Fe, 27 wt.% Re, up to 1 wt.% Os, below the detection limit of Pt. The solubility of rhenium in the Ms melt, corresponding to saturation, is more than 10.0 ± 1.5 and less than 11.6 ± 1.5 wt.%, the carbon content, determined by adding the sum of the analysis to 100 wt.%, is about 4 wt.%.

Relics of rhenium occur in a microcrystalline matrix and massive sulfides and are characterized by wide variations in the contents of Re (61–69 wt.%) and Fe (28–36 wt.%), contain up to 2 wt.% Os, below the detection limit of Pt. The Fe metal phase at the contact with rhenium relics contains 86–90 wt.% Fe and 7–10 wt.% Re. The close paragenesis of rhenium relics with metallic Fe in the sulfide matrix is due to redox reactions between the sulfide melt and metallic rhenium with the reduction of the ^{+2}Fe ion of the sulfide melt to a metallic one: $^{+2}\text{Fe}(\text{Ms}) + 2e = {}^0\text{Fe}(\text{Mc})$ and the oxidation of metallic rhenium: ${}^0\text{Re}(\text{Ms}) - 2e = ^{+2}\text{Re}(\text{Ms})$ to 2 or 4 valence ion.

A sensitive indicator of the processes of accretion of terrestrial planets and the formation of their metallic cores is the distribution of Fe, Co, Ni, Re, Os, Pt between Mc and Ms melts. The fact is that Re, Os, Pt are both strongly siderophile and strongly chalcophile elements, since in the associations silicate (Sil) - Mc melts or Sil - Ms melts, these elements are effectively concentrated in both Mc and Ms melts with separation factors D Mc/Sil and D Ms/Sil reaching 3 or more orders of magnitude (Liu and Fleet, 2001; Bezmen N.I. et al., 1994). In addition, the Mc and Ms distributions of Re, Os, Pt are of interest given the genetic significance of the $^{187}\text{Re}/^{187}\text{Os}$ and $^{190}\text{Pt}/^{186}\text{Os}$ isotope ratios based on the β -decay of ^{187}Re to ^{187}Os and the α -decay of ^{190}Pt to ^{186}Os during the early differentiation of cosmic bodies and meteorites. According to the same parameters, Fe, Co, Ni are both moderately siderophile and moderately chalcophile elements with D Mc/Sil and D Ms/Sil on the order of $n \cdot 10^2$ (Rajamani and Naldrett, 1978). Explanation of the behavior of these elements during Mc and Ms liquation of a sulfide melt is of interest for understanding the geochemistry of the Mc-Ms liquation in the Fe-S-C system and assessing the chalcophile and siderophile properties of these elements.

Table 2 shows the representative compositions of Mc and Ms melts, separation coefficients of ore elements, and distribution coefficients of Re/Os and Pt/Os between Mc and Ms melts.

In the Re-Os association, rhenium is a more siderophilic element, D Mc/Ms = 12.64 than osmium, D Mc/Ms = 1.51. High values of D (Mc/Ms) Re with respect to D (Mc/Ms) Os and high values of the distribution coefficient Kd (Mc/Ms) Re/Os (8.37) indicate effective fractionation of Re relative to Os during Mc-Ms separation sulfide melt due to the redistribution of Re into the Fe-metal phase. This effect will lead to a decrease in the Re/Os and $^{187}\text{Re}/^{187}\text{Os}$ ratios in the coexisting sulfide melt.

In the Pt-Os association, osmium is a siderophile element in terms of the separation coefficients Kd (Mc/Ms) Os and Pt (1.51 and 0.62, respectively), while Pt is a chalcophile element.

Considering the close separation coefficients of Re, Os, and Pt between the silicate, Mc, and Ms melts, it is obvious that their relative concentrations in the silicate melt will be the same in the coexisting Mc and Ms melts.

Co and Ni, according to the same parameters as Re, Os, Pt, are both moderately siderophile and moderately chalcophile elements with D Mc/Sil and D Ms/Sil on the order of $n \cdot 10^2$. The distribution of Co and Ni between Mc and Ms melts is similar to the distribution of Pt and Os. Based on D (Mc / Ms) Co (1.60) and Ni (0.92), the siderophile element is Co,

and the chalcophile element is Ni. However, the values of D (Ms/Ms) for both Co and Ni close to 1 indicate the absence of effective fractionation of Co and Ni in the distribution between Ms and Ms melts in settings with metal sulfide separation in the basalt–Fe–S–C system.

Thus, the behavior of Re, Co, Ni, Os, and Pt during metal-sulfide separation of sulfide melt in the basalt–FeS–Fe–C system is different. Close to 1 D Mc/Ms Co, Ni, Os, and Pt indicate the absence of their noticeable fractionation in the distribution between Mc and Ms melts. At the same time, high values of D Mc/Ms Re indicate efficient fractionation of Re due to redistribution into the Mc melt. Fractionation of Re during metal-sulfide liquation in the basalt–Fe–S–C system will lead to a change in the Re/Os and $^{187}\text{Re}/^{187}\text{Os}$ ratios in the coexisting silicate, Fe-metal, and Fe-sulfide melts. Minor variations in Pt/Os and $^{190}\text{Pt}/^{186}\text{Os}$ ratios in coexisting Mc, Ms and Sil melts, indicating the absence of effective fractionation of Os and Pt in the distribution between Mc, Ms and Sil melts and will not significantly change the Pt/Os and $^{190}\text{Pt}/^{186}\text{Os}$ ratios between coexisting silicate, metallic, and sulfide melts in environments with metal-sulfide liquation.

This study is fulfilled under Research program FMUF-2022-0001_of the Korzhinski Institute of Experimental Mineralogy, supported by RSF grant No. 21-17-00119.

References

- Gorbachev N.S., Shapovalov Yu.B., Kostyuk A.V., Gorbachev P. N., Nekrasov A.N., Sultanov D.M. Phase relations in the Fe-S-C system at P=0.5 GPa, T=1100–1250°C: Fe-S-C liquation and its role in the formation of magmatic sulfide deposits // *Doklady Earth Science*, 2021, Vol. 497(1), p. 206-210
- Litvin Yu.A. Physico-chemical studies of the melting of the deep matter of the Earth. M.: Science. 1991. 312 C.
- Sorokhtin O. G., Ushakov S. A. Global evolution of the Earth. Moscow publishing house. university 1991 446 p.
- Bezmen N. I. et al. Distribution of Pd, Rh, Ru, Jr, Os, and Au between sulfide and silicate metals // *Geochimica et Cosmochimica Acta*. 1994. T. 58. №. 4. C. 1251-1260.
- Gorbachev N.S. Fluid-magma interaction in sulfide-silicate systems // *International Geology Review*. 1990. V. 32. №. 8. P. 749-836.
- Halliday A. N., Wood B. J. How did Earth accrete? // *Science*, 2009. T. 325. №. 5936. C. 44-45.
- Li J., Agee C.B. Pressure effect on partitioning of Ni, Co, S: implications for mantle-core formation // *Lunar and Planetary Science Conference*. 1996. T. 27.
- Liu M. and Fleet M.E. Partitioning of siderophile elements (W, Mo, As, Ag, Ge, Ga, and Sn) and Si in the Fe–S system and their fractionation in iron meteorites. *Geochim. Cosmochim. Acta* 65. 2001. 671–682.
- McDonough W.F., Sun S. The composition of the Earth. *Chem Geol*. 1995. 120, 223–253.
- Rajamani V., Naldrett A. J. Partitioning of Fe, Co, Ni, and Cu between sulfide liquid and basaltic melts and the composition of Ni-Cu sulfide deposits // *Economic Geology*. 1978. T. 73. №. 1. C. 82-93.

Iskrina A.V.^{1,2}, Bobrov A.V.^{1,2,3}, Spivak A.V.², Kuzmin A.V.⁴, Chariton S.⁵, Fedotenko T.⁶ Dubrovinsky L.S.⁷ Postspinel phases at the conditions of the Earth's transition zone and lower mantle. UDC: 549.02

¹Lomonosov Moscow State University, Moscow, ²D.S. Korzhinskii Institute of Experimental Mineralogy RAS, Chernogolovka, ³Vernadsky Institute of Geochemistry and Analytical Chemistry RAS, Moscow, ⁴Institute of Solid State Physics RAS, Chernogolovka, ⁵Center for Advanced Radiation Sources, University of Chicago, Chicago, ⁶Deutsches Elektronen-Synchrotron (DESY), Hamburg, Germany, ⁷Bavarian Research Institute of Experimental Geochemistry and Geophysics (BGI) Bayreuth, Germany (iskrina@iem.ac.ru)

Abstract. Spinel is a widespread mineral, however, the area of its stability is limited, and at great depths there is a transformation into the so-called post-spinel phases. Phases with structures of calcium ferrite (CF), calcium titanate (CT) and marokite are considered as the main candidates for the role of post-spinel phases. Natural post-spinel phases have a complex composition. Structures with a "marokite" channel can include various cations, e.g. Cr, Al, Mg, Fe, Ca, Ti, Fe, Na, while forming solid solutions. High-pressure post-spinel phases have been found as inclusions in diamonds, meteorites, and impact craters. Experimental studies have determined the conditions of formation, the boundaries of phase transitions and changes in the physical properties of post-spinel phases in various chemical systems over a wide range of pressures and temperatures. In this study we report on natural and experimental post-spinel phases of various structures, their solid solutions and stability areas.

Keywords: *post-spinel phases, transition zone, lower mantle, structure, "marokite" channel, phase relations*

Spinel is a widespread mineral found in various geological environments. Most spinels decompose to oxides at high pressure (Reid and Ringwood, 1969) or undergo structural phase transitions. Phases with structures of calcium ferrite (CF), calcium titanate (CT) and marokite are considered as the main candidates for the role of post-spinel phases (Decker and Kasper, 1957, Rogge et al., 1998, Giesber et al., 2001). The structures with a centered *Cmcm* (*Bbmm*) and primitive *Pnma* (*Pmcn*), *Pbcm* (*Pmab*) cells are distinguished within this family of topologically related structures with a "marokite" channel formed by six octahedra.

Unfortunately, at present, post-spinel phases, their properties, and the ability to form the series of

solid solutions have not been sufficiently studied. This paper reports on natural and experimental varieties of post-spinel phases with various structures, their solid solutions and stability areas.

In nature, post-spinel phases can be both high-pressure and low-pressure phases. High-pressure post-spinel phases have been found as inclusions in diamonds, meteorites, and impact craters. Polymineral assemblages were found as inclusions in superdeep diamonds from the Juina-5 kimberlite (Brazil). It containing iron carbide aggregate, Fe-rich periclase, graphite, orthorhombic $\text{Mg}(\text{Cr},\text{Fe})_2\text{O}_4$ oxide and orthorhombic CaCr_2O_4 oxide (Kaminsky et al., 2015).

In the study Walter et al. (2011), several high-pressure phases were described: a phase with a CF structure; a new hexagonal aluminum phase (NAL); Al, Ti and Fe-containing Mg-perovskite; and Ti-rich Ca-perovskite. Maohokite (MgFe_2O_4), a post-spinel polymorph of magnesioferrite with a CF-type structure (*Pnma*) (Chen et al., 2019); xieite (FeCr_2O_4) – a natural orthorhombic polymorph of chromite with a calcium ferrite-type structure (Chen et al., 2008); chenmingite (FeCr_2O_4) – a high-pressure mineral with a CF-structure (*Pnma*) (Ma et al., 2019); tschaunerite ($\text{Fe}^{2+}(\text{Fe}^{2+}\text{Ti}^{4+})\text{O}_4$) is a high-pressure polymorph of the ulvöspinel with a CT-type structure (Ma, Prakapenka, 2018).

Experimental studies have determined the conditions of formation, the boundaries of phase transitions and changes in the physical properties of post-spinel phases in various chemical systems over a wide pressures and temperatures range. The studied phases can be divided into several groups: $A^{2+}\text{Fe}^{3+}_2\text{O}_4$; $A^{2+}\text{Cr}^{3+}_2\text{O}_4$; $A^{2+}\text{Al}^{3+}_2\text{O}_4$ и $A^{2+}\text{Mn}^{3+}_2\text{O}_4$, where the A^{2+} position is occupied by various cations, for example, Ca, Mg, Fe, Mn, Zn, Co, etc. There is also a group with another stoichiometry $A^{2+}_2B^{4+}\text{O}_4$, where Ti occupies position B^{4+} , and Fe, Zn, Co can be located in position A^{2+} (Iskrina et al., 2022 and references therein).

Some systems of solid solutions of post-spinel phases have been experimentally studied as well: MgAl_2O_4 - Mg_2SiO_4 (Kojitani et al., 2007); MgAl_2O_4 - CaAl_2O_4 (Akaogi et al., 1999); NaAlSiO_4 - MgAl_2O_4 (Ono et al., 2009); Mg_2SiO_4 - MgCr_2O_4 (Bindi et al., 2018).

An MgAl_2O_4 – Mg_2SiO_4 solid solution was studied up to ~27 GPa and $T=1600^\circ\text{C}$ (Kojitani et al., 2007). In the pressure range >23 GPa, the CF phase appears in the assemblages. When the MgAl_2O_4 content exceeds ~23 mol%, only the CF phase remains in the system at a pressure above 26.5 GPa. An MgAl_2O_4 - CaAl_2O_4 solid solution was studied up to ~26 GPa and $T=1200^\circ\text{C}$ (Akaogi et al., 1999). At pressures above 8 GPa, the CA-IV phase transforms into a phase with the calcium ferrite-type structure.

The MgAl_2O_4 compound transforms into a CF-phase at 26-27 GPa and is in association with the hexagonal aluminum phase (*Hex.P*). An NaAlSiO_4 - MgAl_2O_4 solid solution was studied up to ~30 GPa and $T=1600^\circ\text{C}$ (Ono et al., 2009). At pressures above ~17 GPa, the $\text{NaAlSi}_2\text{O}_6$ *Jd* phase decomposes to form the NaAlSiO_4 phase with a calcium ferrite-type (CF) structure. This phase is stable up to the extreme pressures studied in this work of 30 GPa, only if the admixture of the Mg component does not exceed 30 mol.%. With a greater entry of magnesium into the NaAlSiO_4 structure, in addition to the CF phase, a hexagonal aluminum phase *Hex.P*. is also formed. In the study Bindi et al. (2018) the chromium-containing ringwoodite (4.23 wt.% Cr_2O_3) with reversed structure was synthesized at a pressure of 20 GPa and a temperature of 1600°C in the Mg_2SiO_4 - MgCr_2O_4 system. $\text{Mg}(\text{Mg},\text{Cr},\text{Si})_2\text{O}_4$ with a distorted orthorhombic CT structure obtained in the study Sirotkina et al. (2018) in a wide pressure range (13-18 GPa) during the experimental study of the Mg_2SiO_4 - MgCr_2O_4 model system is considered as the phase due to which a high-pressure modification $(\text{Mg},\text{Fe})_2\text{SiO}_4$ is formed. In this system at a pressure of 16 GPa and 1600°C , a solid solution of $\text{Mg}[(\text{Cr},\text{Mg})(\text{Si},\text{Mg})]\text{O}_4$ was obtained as well. It has a distorted CT structure and the *Cmc2*₁ space group (Bindi et al., 2015).

The findings of post-spinel phases among inclusions in deep diamonds and their association with other mantle minerals supports the possibility of their formation in diamond-forming area and the presence in deep layers of the Earth. A wide range of their composition, indicates that they may be considered as host-phases for aluminum, alkalis and a number of impurity elements at high temperatures and pressures corresponding to the transition zone and the lower mantle of the Earth (Irifune and Ringwood, 1993; Kesson et al., 1994; Perrillat et al., 2006).

This study was supported by the Russian Foundation for Basic Research, project №20-35-90095\20. This study carried out within the scientific plan of the Laboratory of deep geospheres of the Lomonosov Moscow state University and within the Research Program of the D.S. Korzhinskii Institute of Experimental Mineralogy Russian Academy of Sciences (FMUF-2022-0001).

References

1. Akaogi M., Hamada Y., Suzuki T., Kobayashi M. and Okada M. (1999) High pressure transitions in the system MgAl_2O_4 - CaAl_2O_4 : A new hexagonal aluminous phase with implication for the lower mantle. *Phys. Earth Planet. Inter.* 115, 67–77.
2. Bindi L., Sirotkina E. A., Bobrov A. V. and Irifune T. (2015) Letter. Structural and chemical characterization of $\text{Mg}[(\text{Cr},\text{Mg})(\text{Si},\text{Mg})]\text{O}_4$, a new

- post-spinel phase with sixfold-coordinated silicon. *Am. Mineral.* 100, 1633–1636.
3. Bindi L., Griffin W.L., Panero W.R., Sirotkina E., Bobrov A., Irifune T. (2018) Synthesis of inverse ringwoodite sheds light on the subduction history of Tibetan ophiolites. *Sci. Rep.* 8, 5457.
 4. Chen M., Shu J. F. and Mao H. K. (2008) Xieite, a new mineral of high-pressure FeCr_2O_4 polymorph. *Chinese Sci. Bull.* 53, 3341–3345.
 5. Chen M., Shu J., Xie X. and Tan D. (2019) Maohokite, a post-spinel polymorph of MgFe_2O_4 in shocked gneiss from the Xiuyan crater in China. *Meteorit. Planet. Sci.* 54, 495–502.
 6. Decker B. F. and Kasper J. S. (1957) The structure of calcium ferrite. *Acta Crystallogr.* 10, 332–337.
 7. Giesber H. G., Pennington W. T. and Kolis J. W. (2001) Redetermination of CaMn_2O_4 . *Acta Crystallogr. Sect. C Cryst. Struct. Commun.* 57, 329–330.
 8. Irifune T. and Ringwood A. E. (1993) Phase transformations in subducted oceanic crust and buoyancy relationships at depths of 600–800 km in the mantle. *Earth Planet. Sci. Lett.* 117, 101–110.
 9. Iskrina A.V., Bobrov A.V., Spivak A.V. (2022) Post-spinel phases in the Earth's mantle. *Geochemistry International.* 60, 4, 311–324.
 10. Kaminsky F. V., Wirth R. and Schreiber A. (2015) A microinclusion of lower-mantle rock and other minerals and nitrogen lower-mantle inclusions in a diamond. *Can. Mineral.* 53, 83–104.
 11. Kesson S. E., Gerald J. D. F. and Shelley J. M. G. (1994) Mineral chemistry and density of subducted basaltic crust at lower-mantle pressures. 372, 767–769.
 12. Kojitani H., Hisatomi R. and Akaogi M. (2007) High-pressure phase relations and crystal chemistry of calcium ferrite-type solid solutions in the system $\text{MgAl}_2\text{O}_4\text{-Mg}_2\text{SiO}_4$. *Am. Mineral.* 92, 1112–1118.
 13. Ma C. and Prakapenka V. (2018) Tschaunerite, IMA 2017-032a. *CNMNC Newsletter No. 46*, December 2018, page 1188. *Eur. Mineral.* 30, 1181–1189.
 14. Ma C., Tschauner O., Beckett J. R., Liu Y., Greenberg E., Prakapenka V. B. (2019) Chenmingite, FeCr_2O_4 in the CaFe_2O_4 -type structure, a shock-induced, high-pressure mineral in the Tissint martian meteorite. *Am. Mineral.* 104 (10), 1521–1525.
 15. Ono A., Akaogi M., Kojitani H., Yamashita K. and Kobayashi M. (2009) High-pressure phase relations and thermodynamic properties of hexagonal aluminous phase and calcium-ferrite phase in the systems $\text{NaAlSiO}_4\text{-MgAl}_2\text{O}_4$ and $\text{CaAl}_2\text{O}_4\text{-MgAl}_2\text{O}_4$. *Phys. Earth Planet. Inter.* 174, 39–49.
 16. Perrillat J., Daniel I., Fiquet G., Mezouar M. and Guignot N. (2006) Phase transformations of subducted basaltic crust in the uppermost lower mantle. 157, 139–149.
 17. Reid A. F. and Ringwood A. E. (1969) Newly observed high pressure transformations in Mn_3O_4 , CaAl_2O_4 , and ZrSiO_4 . *Earth Planet. Sci. Lett.* 6, 205–208.
 18. Rogge M. P., Caldwell J. H., Ingram D. R., Green C. E., Geselbracht M. J. and Siegrist T. (1998) A New Synthetic Route to Pseudo-Brookite-Type CaTi_2O_4 . *J. Solid State Chem.* 141, 338–342.
 19. Sirotkina E.A., Bobrov A.V., Bindi L., Irifune T. (2018) Chromium-bearing phases in the Earth's mantle: Evidence from experiments in the $\text{Mg}_2\text{SiO}_4\text{-MgCr}_2\text{O}_4$ system at 10–24 GPa and 1600°C. *Am. Miner.* 103, 151 – 160.
 20. Walter M. J., Kohn S. C., Araujo D., Bulanova G. P., Smith C. B., Gaillou E., Wang J., Steele A. and Shirey S. B. (2011) Deep mantle cycling of oceanic crust: Evidence from diamonds and their mineral inclusions. *Science* (80). 334, 54–57.

Ivanov M.V. Equation of state and thermodynamic properties of the fluid system $\text{H}_2\text{O} - \text{CO}_2 - \text{NaCl} - \text{CaCl}_2$ at P - T parameters of the middle and lower crust. UDC: 550.41+536.7

IPGG RAS, St. Petersburg (m.v.ivanov@ipgg.ru)

Abstract. Based on the earlier obtained equations of state for ternary systems $\text{H}_2\text{O-CO}_2\text{-CaCl}_2$ and $\text{H}_2\text{O-CO}_2\text{-NaCl}$ (Ivanov, Bushmin, 2019, 2021), an equation of state for the four-component fluid system $\text{H}_2\text{O-CO}_2\text{-NaCl-CaCl}_2$ is derived in terms of the Gibbs excess free energy. A corresponding numerical thermodynamic model is build. The most of the numerical parameters of the model coincide with corresponding parameters of the ternary systems. A parameter for NaCl-CaCl_2 interaction is obtained from the experimental liquidus for the mixture of salts. The model is valid for pressures of 1–20 kbar and temperatures from 500°C to 1400°C. The model allowed to carry out a detailed study of the phase state and activities of water in sections $\text{H}_2\text{O-CO}_2\text{-salt}$ at variations of the ratio $x_{\text{NaCl}}/(x_{\text{NaCl}}+x_{\text{CaCl}_2})$. Due to removal of restrictions resulting from a smaller number of components in ternary systems, the thermodynamic behavior of systems with a mixed composition of the salt is significantly differ from the behavior of those with a single salt component.

Keywords: high temperature, high pressure, fluid, four-component system, phase splitting, CO_2 , NaCl , CaCl_2

Deep aqueous fluids play an important role in the crustal petrogenesis and in transportation of deep-seated matter to the upper crust. Aqueous fluids usually contain chlorides of alkali and alkali-earth metals and dissolved non-polar gases, in particular CO_2 . With ascent to the surface, the pressure and temperature of deep fluids significantly change, which results in substantial transformation of their physical-chemical characteristics. In particular, an effect of lowering pressure can be splitting of homogeneous fluid into immiscible fluid phases, contrasting in their physical and chemical properties. In our previous works (Ivanov, Bushmin, 2019, 2021), we have developed numerical thermodynamic models for two ternary fluid systems with components: water, CO_2 , and salt. Both models are valid for temperatures from 500°C to 1400°C and pressures from 1 kbar to 20 kbar. The models were

developed for salts NaCl (Ivanov, Bushmin, 2021) and CaCl₂ (Ivanov, Bushmin, 2019). The both salts are the most abundant salts in crustal fluids (Liebscher, 2007). For the both ternary systems with a single salt we studied in detail the dependencies of their physical-chemical characteristics on the pressure, temperature, and composition of the system (phase diagrams, activities of components, density of the fluid). However, some features of *natural fluids* can be missed in this investigation, first of all, because natural fluids usually consist of more than three components. This relates, first, to their non-gaseous part, which is usually has more complex composition, in particular, being a mixture of several

salts. The presence of several salts can result in appearance some features in the properties of the fluid system absent or different from that of systems with pure salts. In this communication, we present a numerical thermodynamic model of a four-component fluid system H₂O-CO₂-NaCl-CaCl₂, which is a natural extension of our models for systems H₂O-CO₂-NaCl and H₂O-CO₂-CaCl₂.

Our form of the Gibbs excess free energy for the four-component fluid system G^{mix} contains the same terms for interactions between species and follows the same approach for the entropy dependent part of the free energy as in works (Ivanov, Bushmin, 2019, 2021). In terms of mole fractions of the components,

$x_1 = x_{\text{H}_2\text{O}}$, $x_2 = x_{\text{CO}_2}$, $x_3 = x_{\text{NaCl}}$, $x_4 = x_{\text{CaCl}_2}$, $x_1 + x_2 + x_3 + x_4 = 1$, it looks like

$$\begin{aligned}
 G^{\text{mix}} = & RT \{ (1-x_2) \ln(1-x_2) - [x_1 + (1+\alpha_3)x_3 + (1+\alpha_4)x_4] \ln[x_1 + (1+\alpha_3)x_3 + (1+\alpha_4)x_4] + \\
 & + x_1 \ln x_1 + x_2 \ln x_2 + (1+\alpha_3)x_3 \ln[(1+\alpha_3)x_3] + (1+\alpha_4)x_4 \ln[(1+\alpha_4)x_4] \} \\
 & + W_{12}x_1x_2(x_1+x_2)/(V_1x_1+V_2x_2) \\
 & + W_{13}x_1x_3 + W_{14}x_1x_4 + W_{34}x_3x_4 \\
 & + x_2x_3[x_2W_{23} + x_3W_{32}]/(x_2+x_3) + x_2x_4[x_2W_{24} + x_4W_{42}]/(x_2+x_4) \\
 & + W_{123}x_1x_2x_3 + W_{124}x_1x_2x_4
 \end{aligned} \tag{1}$$

Quantities α_i are the numbers of additional particles, formed by dissociation of corresponding molecules $0 \leq \alpha_3 \leq 1$, $0 \leq \alpha_4 \leq 2$. V_1 and V_2 are the molar volumes of pure water and carbon dioxide at a given temperatures and pressures. At $x_3 = 0$ or $x_4 = 0$ Eq. (1) turns into equations for ternary systems H₂O-CO₂-CaCl₂ (Ivanov, Bushmin, 2019) or H₂O-CO₂-NaCl (Ivanov, Bushmin, 2021). The parameters W_{ij} and W_{ijk} in the Eq. (1) are supposed to be dependent on the temperature T and pressure P , but independent on the mole fractions of the components. The form of P - T dependences of parameters W_{ij} , W_{ijk} and corresponding numerical values for ternary systems are given in the cited works. These parameters, fitted on experimental data on fluids H₂O-CO₂-NaCl and H₂O-CO₂-CaCl₂, are retained in the thermodynamic model of the four-component fluid system, presented here. The full Gibbs free energy for the system H₂O-CO₂-NaCl-CaCl₂, which can contain coexisting fluid phases and phases of solid salts, includes corresponding terms of the form Eq. (1) and terms describing solid-liquid transitions for pure salts (Ivanov, Bushmin, 2019, 2021).

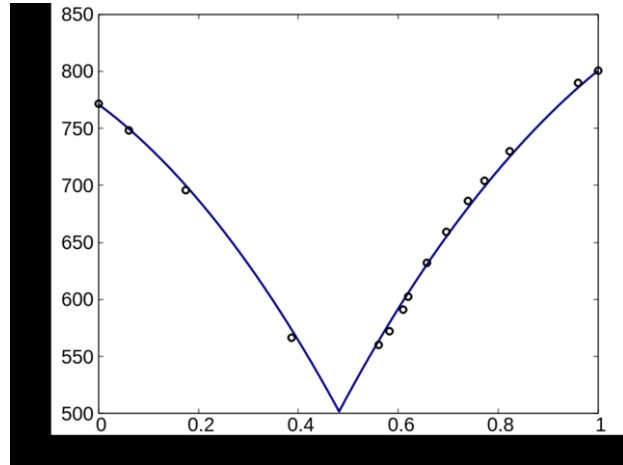


Fig. 1. Liquidus of the system NaCl-CaCl₂ at $P = 1$ bar in our model (line). Circles are experimental results by (Seltveit, Flood, 1958).

The only new parameter in the model of the four-component system not obtained in previous works is W_{34} , which describes the effect of the interaction of species NaCl and CaCl₂ in the fluid. In the case $x_1 = x_2 = 0$, Eq. (1) retains only the entropy terms (first two lines of Eq. (1)) and the term $W_{34}x_3x_4$. In this case Eq. (1) appears to be an equation of state of a molten mixture of NaCl and CaCl₂. With terms describing solid-liquid transitions of the salts, this should describe solid-liquid phase transition in the mixture of salts. Experimental data on the liquidus in this system are well known for $P = 1$ bar (Seltveit, Flood, 1958; Chartrand, Pelton, 2001). The liquidus has a simple shape, typical for mixtures with no

intermediate compounds. For $P=1$ bar and temperatures above 500°C , our equations give $\alpha_3 = \alpha_4 = 0$. This provides a common form of the entropy-dependent terms in the free energy of mixing of two substances NaCl and CaCl_2 . Thus, Eq. (1) together with known equations for melting of the pure salts is valid for obtaining liquidus in the mixture NaCl- CaCl_2 . This circumstance permits obtaining the value of the parameter W_{34} based on experimental data. In Fig. 1 the liquidus,

built with our equation of state at $W_{34}=-10.3\text{kJ/mol}$, is compared with experimental data by (Seltveit, Flood, 1958). At $W_{34}=-10.3\text{kJ/mol}$, the eutectic point corresponds to the temperature 502°C and $x_{\text{NaCl}}=0.482$. This is in a full agreement with numerous experimental data (Chartrand, Pelton, 2001). The value of W_{34} along with parameters obtained in (Ivanov, Bushmin, 2019, 2021) form a full set of parameters of our thermodynamic model of the four-component system $\text{H}_2\text{O}-\text{CO}_2-\text{NaCl}-\text{CaCl}_2$.

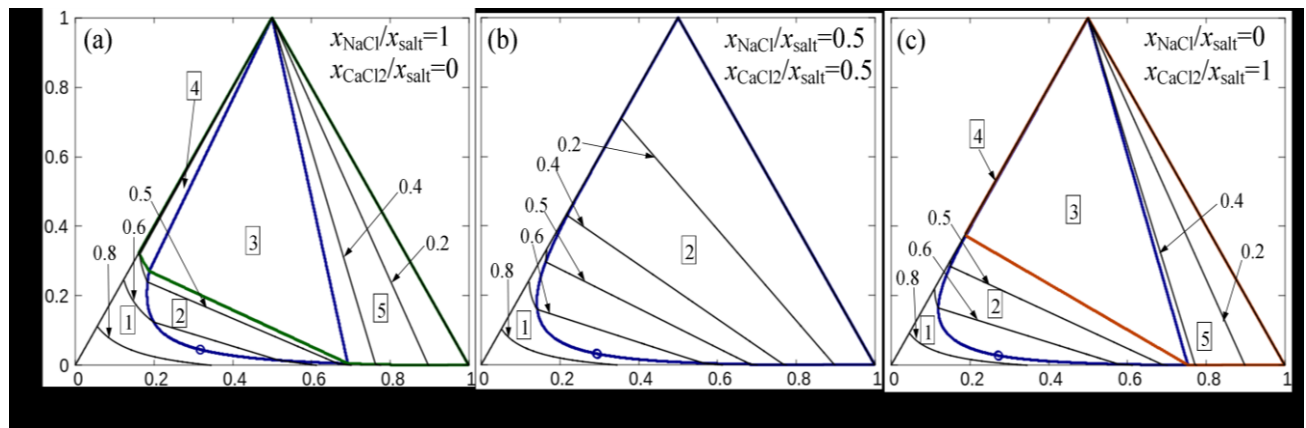


Fig. 2. Evolution of phase diagrams of the system $\text{H}_2\text{O}-\text{CO}_2\text{-salt}$ at variations of the ratio $x_{\text{NaCl}}/(x_{\text{NaCl}}+x_{\text{CaCl}_2})$, $x_{\text{salt}}=x_{\text{NaCl}}+x_{\text{CaCl}_2}$. $T=500^{\circ}\text{C}$, $P=5$ kbar. The bold blue line is the border of the field of coexistence of two fluid phases (solvus). The open circle indicates the critical point in the region of the two-phase fluid. Bold green and orange lines are borders of regions of existence of solid phases of NaCl and CaCl_2 correspondingly. The numbers in boxes indicates areas (fields) of different phase compositions: 1 – homogeneous fluid; 2 – two coexisting fluid phases; 3 – two fluid phases coexisting with solid salt ((a) – NaCl and (c) – CaCl_2); 4 – brine coexisting with solid salt; 5 – CO_2 rich fluid coexisting with solid salt. Thin black lines are isolines of chemical activity of water. The numbers with arrows show corresponding values of the activity.

It is convenient to present results, obtained with our model of four-component system with two salts, in a form, similar to that usual for ternary systems with one salt component, i.e. to consider phase diagrams in coordinates $x_{\text{H}_2\text{O}}-x_{\text{CO}_2}-x_{\text{salt}}$, where $x_{\text{salt}}=x_{\text{NaCl}}+x_{\text{CaCl}_2}$, for fixed ratios $r_{\text{salt}}=x_{\text{NaCl}}/x_{\text{salt}}$ in the total composition of the system. Three phase diagrams of such kind for $T=500^{\circ}\text{C}$ and $P=5$ kbar are presented in Fig. 2. The edge ternary systems Fig. 2a and Fig. 2c show a complex phase picture of five different fields: 1. Homogeneous fluid; 2. Two coexisting fluid phases; 3. Two fluid phases coexisting with solid salt; 4. Brine coexisting with solid salt; 5. CO_2 rich fluid coexisting with solid salt. In the broad *field-3*, there are three coexisting phases, which provide fixed values of activities of components in the entire field ($a_{\text{H}_2\text{O}}=0.474$, $a_{\text{CO}_2}=0.742$, $a_{\text{NaCl}}=0.212$ for $r_{\text{salt}}=1$ and $a_{\text{H}_2\text{O}}=0.424$, $a_{\text{CO}_2}=0.779$, $a_{\text{CaCl}_2}=0.343$ for $r_{\text{salt}}=0$). The phase diagram Fig. 2b for the fluid with equal mole fractions of NaCl and CaCl_2 contains only two phase fields, i.e. a field of the homogeneous fluid and a field of two coexisting fluid phases. Comparing to Figs. 2a and 2c, the fields containing solid salt disappear due to better solubility of the salt

of mixed composition comparing its pure constituents. However, the differences between fluids with one pure salt component and mixed salts are more profound.

In Fig. 3 we show how the phase diagram of the fluid system $\text{H}_2\text{O}-\text{CO}_2-\text{CaCl}_2$ changes when adding small portions of the second salt NaCl. The initial phase diagram for the ternary system is present in Fig. 2c. The system in Fig. 3a differs in adding only 0.2% of NaCl to CaCl_2 . The *field-3* of three coexisting phases radically increases, whereas *field-5* of CO_2 rich fluid coexisting with solid salt dramatically shrinks. In Fig. 3a *field-3* is not a region of constant activity of water of $a_{\text{H}_2\text{O}}=0.424$ as in Fig. 2c. Isolines of $a_{\text{H}_2\text{O}}$ cross this field. Activity of water can change in the field of two-phase fluid coexisting with solid salt from 0.423 down to 0. Activities of the other components are also non-constant in this field. On the other hand, adding 0.2% of the second salt has only minor impact on the position of border between *field-2* and *field 3*, i.e. on the concentrations of salt and CO_2 resulting in appearance of a solid salt phase. Changing position of this line requires more sufficient changes in the salt composition as it shown in Fig. 3b.

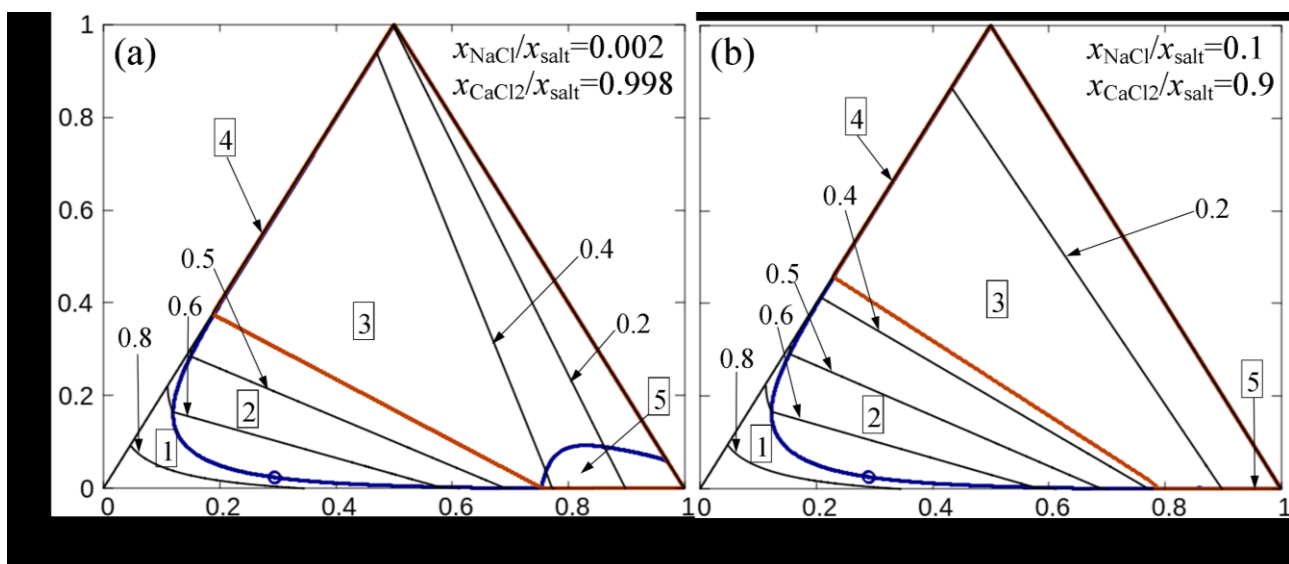


Fig. 3. Changes in phase diagrams when transition between pure and mixed salt. See also Fig. 2 for notations.

Another major difference between ternary and four-component fluid systems is associated with the composition of coexisting fluid phases. In ternary systems water-gas-salt the isolines of activity of components are curves in the field of a homogeneous fluid. If they cross the solvus and enter the field of two coexisting fluids, they turn into straight lines, the tie lines, connecting two points of the intersections with the solvus. The compositions of two coexisting fluid phases along the tie line are constant. One of this phases has a composition of the homogeneous fluid at the upper point of crossing. The composition of another phase coincides with the composition homogeneous fluid at the lower crossing point. In the four-component fluid, a difference in energetics of interaction of NaCl and CaCl₂ with water and CO₂ results in redistribution of salts between coexisting fluid phases. In result, the compositions of coexisting fluid phases are not constant along the isolines of constant activities. They are not tie lines in four-component systems, and they are not straight lines in general. An example of the redistribution of salt component along a line of a constant activity is given in Fig. 4. In this plot, we separately present the ratio r_{salt} for two coexisting fluid phases along the isoline $a_{\text{H}_2\text{O}} = 0.6$ in Fig. 2b (the total composition of the system corresponds to $r_{\text{salt}} = 0.5$) as a function of the mole fraction of CO₂. For the homogeneous fluid, $r_{\text{salt}} = 0.5$. After the isoline crosses the solvus at $x_{\text{CO}_2} = 0.102$, a second fluid phase appears (green curve). This phase is in equilibrium with the initial one at $a_{\text{H}_2\text{O}} = 0.6$, but the ratio of the salt mole fractions in it is very different from the total r_{salt} . The second phase is more rich in NaCl due to a minor loss of NaCl in the initial fluid (blue line). The total ratio in two fluids always remain $r_{\text{salt}} = 0.5$. When following along the isoline two fluid phases

exchange salts and other components. Finally at $x_{\text{CO}_2} = 0.563$ the initial fluid phase disappears and the second fluid acquires the ratio of salt mole fractions corresponding to $r_{\text{salt}} = 0.5$ of the homogeneous fluid.

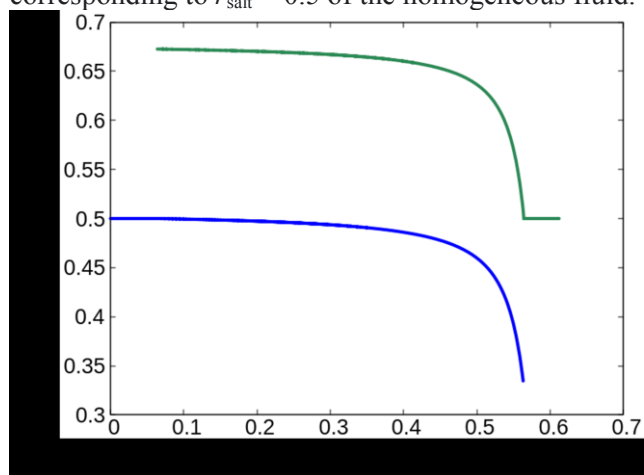


Fig. 4. Ratio $x_{\text{NaCl}}/(x_{\text{NaCl}}+x_{\text{CaCl}_2})$ in coexisting fluid phases along the isoline $a_{\text{H}_2\text{O}} = 0.6$ at $T = 500^\circ\text{C}$, $P = 5$ kbar, and total ratio $x_{\text{NaCl}}/(x_{\text{NaCl}}+x_{\text{CaCl}_2}) = 0.5$ (Fig. 2b).

A summary the presented above is as follows: **1.** An equation of state for the fluid system H₂O-CO₂-NaCl-CaCl₂ expressed in terms of the excess Gibbs free energy of mixing is obtained for temperatures from 500°C to 1400°C and pressures from 1 kbar to 20 kbar; **2.** The most of numerical parameters of the equation were obtained in earlier studies of the edge systems H₂O-CO₂-NaCl and H₂O-CO₂-CaCl₂; **3.** The parameter for NaCl-CaCl₂ interaction is obtained from the experimental data on the liquidus of mixtures of these salts; **4.** The equation of state allows obtaining the most of thermodynamic characteristics of the system for arbitrary mole fractions of the components; **5.** In this paper we

present a series of phase diagrams of the system. Each phase diagram relates to a fixed ratio of the total mole fractions of NaCl and CaCl₂ in the system. These phase diagrams, looking similar to these for ternary systems, make it possible to trace changes in thermodynamics of the system H₂O-CO₂-salt when changing the composition of the salt. Along with features dependent on the properties of the pair NaCl-CaCl₂ and the specifics of our model, this study allows reveal fundamental differences between ternary and four-component systems; **6.** At given P and T both in ternary and four-component systems, there are upper limits for the chemical activity of water in the field of two coexisting fluid phases. When the P - T conditions allow presence of a phase of solid salt, this phase buffers activities of components in ternary systems, which results in appearance of lower limit of activity of water in the field of two coexisting fluid phases. This does not take place in four-component fluid systems with two salts. Even a minor admixture of a second salt with different thermodynamic properties destroys the buffering ability of the solid salt phase. The activity of water in the two-fluid region of mixed-salt four component system can drop down to zero; **7.** In the field of the four-component fluid split into two phases, the lines of constant activities cannot be considered as tie lines, i.e. lines of constant compositions of coexisting phases. A motion along these lines leads to a redistribution of components between the coexisting phases.

The work was carried out in the framework of the research theme of IPPG RAS FMUW-2021-0002.

References

- Chartrand P., Pelton A. D. Thermodynamic equation and optimization of the LiCl-NaCl-KCl-RbCl-CsCl-MgCl₂-CaCl₂ system using the modified quasi-chemical model // *Metall. Mater. Trans. A* 2001. Vol. 32A. P.1361–1383.
- Ivanov M.V., Bushmin S. A. Equation of state of the H₂O-CO₂-CaCl₂ fluid system and properties of fluid phases at P - T parameters of the middle and lower crust // *Petrology*. 2019. V. 27. No. 4. P. 395–406.
- Ivanov M.V., Bushmin S. A. Thermodynamic model of the fluid system H₂O-CO₂-NaCl at P - T parameters of the middle and lower crust // *Petrology*. 2021. V. 29. No. 1. P. 77–88.
- Liebscher A. Experimental studies in model fluid systems // *Rev. Mineral. Geochem.* 2007. Vol. 65(1). P. 15–47.
- Seltveit A., Flood H. Determination of the solidus curve by tracer technique. The system CaCl₂-NaCl // *Acta Chem. Scand.* 1958. Vol. 12. P. 1030–1041.

Kostyuk A.V., Gorbachev N.S., Gorbachev P.N., Nekrasov A.N., Soultanov D.M. Experimental study of melting and phase composition in the basalt-FeS-Fe-C system at $P=4$ GPa, $T=1400^{\circ}$ C. UDC: 550.4.02

Korzhinskii Institute of Experimental Mineralogy RAS. e-mail: nastyu@iem.ac.ru, gor@iem.ac.ru

Abstract. An experimental study of the basalt-FeS-Fe-C system with the parameters of the upper mantle is of interest in connection with the problems of early differentiation of cosmic bodies, the chemical composition of meteorites and magmatic sulfide deposits. The experiments were carried out at the IEM RAS on an anvil with hole type apparatus (NL-40). The quenched sample consisted of ore and silicate parts. The silicate part is composed of products of partial melting of basalt, including restite of eclogitic Grt-Cpx composition with a small amount (< 1%) of intergranular silicate glass of ferrobasalt composition (L₁). The main volume of silicate glass is confined to the ore part of the sample as a result of the injection of basaltic melt (L₂), where it forms extensive areas, mainly in its sulfide part. Like intergranular melts, injection melts are characterized by anomalously high FeO contents (~30 wt.%). The properties of Grt-Cpx restite, the value of the 2-sided contact angle between the crystals corresponded to the conditions of an open system, which contributed to the migration of the main volume of the melt through the intergranular space and its intrusion into the weakened zones of the ore part. During migration and intrusion, the melt captured individual portions of layered sulfide melts.

Keywords: silicate, sulfide, metal, liquation, experiment

Experimental study of the melting and phase composition of the basalt-FeS-Fe-C system is of interest in various areas of research. This is also in connection with the study of the problem of early differentiation of cosmic bodies, and the phase composition of meteorites, as well as magmatic iron-sulfide deposits. We chose the carbon- and sulfur-saturated basalt-FeS-Fe-C system as an experimental model, since in the presence of carbon, the sulfide melt separates into Fe-metal (Mc) and Fe-sulfide (Ms) melts, which are immiscible with the silicate melt. The paper considers some features of the phase relationships and behavior of the silicate melt in the system under study at the parameters of the upper mantle.

The experiments were carried out at the IEM RAS on an anvil with hole apparatus according to the multi-amplular quenching technique (Gorbachev, 1990) at $P=4$ GPa, $T=1400^{\circ}$ C. The temperature was measured with a Pt30Rh/Pt6/Rh thermocouple, and the pressure at high temperatures was calibrated using the quartz-coesite equilibrium. The accuracy of temperature and pressure determination is estimated at $\pm 10^{\circ}$ C and ± 1 kbar (Litvin, 1991). The initial sample consisted of silicate and ore fractions

in a ratio of 1:2 with the addition of metallic Re, Os, and Pt. The silicate part of the original sample consisted of fine powders of silicate glass of magnesian basalt of the Mokulaevskaya suite (mk) of the Norilsk region with the composition (wt.%): SiO₂ 50,02; TiO₂ 1,85; Al₂O₃ 14,51; FeO 14,03; MnO 0,20; MgO 5,85; CaO 10,40; Na₂O 2,50; K₂O 0,72 and the ore part in the ratio of 35 and 65 wt.%, respectively. The ore part consisted of a mixture of

pyrrhotite (58 wt.%), metallic Fe (36 wt.%) and carbon (6 wt.%, in the form of technical carbon P-803). The “sandwich” technique was used, the initial silicate and ore components were layer by layer: ore–silicate–ore samples were loaded into a graphite ampoule, which was also an additional source of carbon. Then it was placed in a Pt ampoule and hermetically sealed.

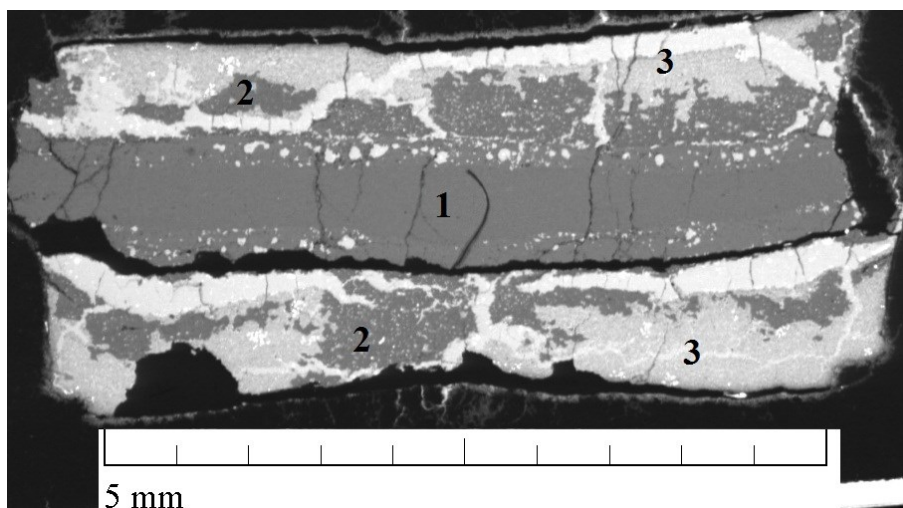


Fig. 1. BSE images of a longitudinal section of the quenched sample. 1 – silicate part, 2 – “injection” segregations of the silicate part in the ore part, 3 – ore part of the sample.

Table 1. Chemical compositions of the coexisting phases of the silicate part.

Oxide/Phase	Gr _t	Cpx	L ₁	L ₂
SiO ₂	38.87 ± 0.50	50.07 ± 0.50	41.73 ± 1.70	42.14 ± 0.64
TiO ₂	1.05 ± 0.31	< n/o	2.54 ± 0.22	1.55 ± 0.15
Al ₂ O ₃	21.55 ± 0.95	8.45 ± 0.67	8.91 ± 0.50	9.94 ± 0.19
FeO	20.95 ± 1.66	13.07 ± 1.38	33.96 ± 1.46	29.46 ± 0.65
MgO	8.38 ± 1.45	10.07 ± 0.22	1.85 ± 0.33	4.25 ± 0.20
CaO	8.45 ± 0.29	15.32 ± 0.42	< n/o	8.29 ± 0.24
Na ₂ O	< n/o	2.29 ± 0.31	3.67 ± 0.98	2.76 ± 0.12
K ₂ O	< n/o	< n/o	< n/o	0.73 ± 0.18
Total	99.25	99.27	92.76	99.12

After the experiment, the hardened sample retained the layered structure inherited from the original “sandwich”, in the center - a silicate part developing along basalt, surrounded from above and below by the quenched ore fraction (Fig. 1).

The silicate part is composed of products of partial melting of basalt, including restite of eclogitic, Gr_t-Cpx composition with intergranular glass – quenched silicate melt. Isolated inclusions of the Fe-sulfide phase are confined to the contact zone of the Gr_t-Cpx restite. Figure 2a shows a BSE images of the silicate part of the polished sample, Table 1 shows the chemical compositions of coexisting phases – garnet, clinopyroxene, and silicate melt.

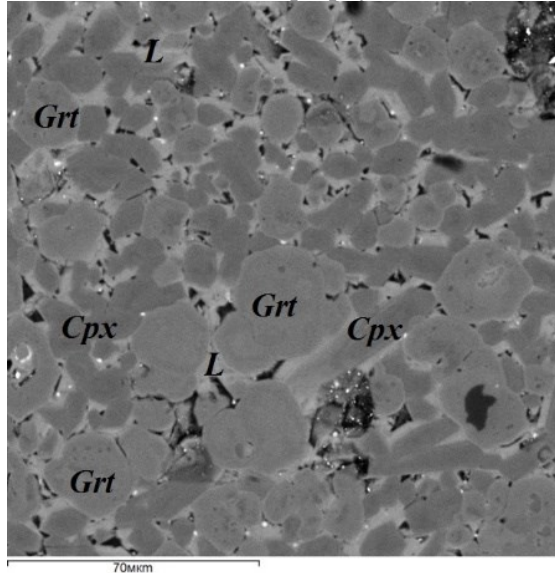
Idiomorphic garnet crystals, 10 to 30 μm in size, alm₆₀-pyr₂₀-gros₂₀ composition (or

$Mg_{1,0}Ca_{0,7}Fe_{1,3}Al_2Si_3O_{12}$), $X_{Mg} = 0.42$, $X_{Ca} = 0.23$, contain ≤ 1 wt % TiO₂ and Cr₂O₃. With regard to the main mineral-forming components – SiO₂, Al₂O₃, MgO, CaO, FeO, garnets are homogeneous. A slight zoning is observed, expressed as a change in the TiO₂ content (from 1.2 to 0.6 wt.%) from the center to the edge of the grain. Clinopyroxenes are represented by tabular segregations of diopside-hedenbergite composition $(Ca_{0,6}Mg_{0,5}Fe_{0,4})(Al_{0,3}Na_{0,1})Si_2O_6$ ranging in size from 10 to 50 μm.

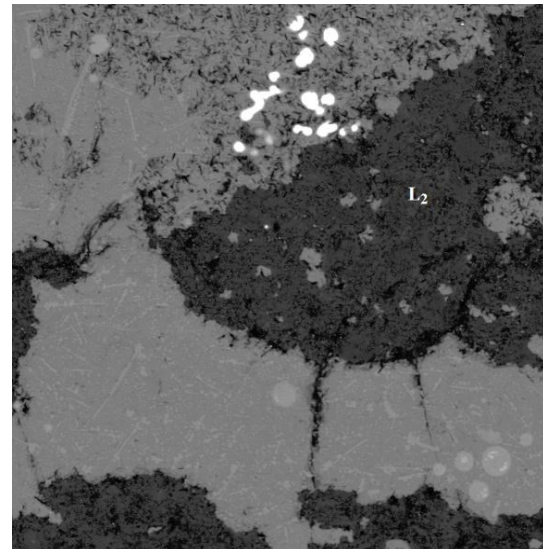
The intergranular space between garnet and clinopyroxenes contains silicate glass formed during quenching of intergranular silicate melt L₁ (Fig. 2a). A distinctive feature of intergranular melts is an increased content of FeO (up to 34 wt.%), alkalis (Na₂O+K₂O up to 6 wt.%), a reduced content of CaO

(up to 5 wt.%) and MgO (up to 2 wt.%). The melts composition is alkaline picobasalts (Table 1).

During the interaction of the silicate fraction with the ore fraction, the basalt melt was introduced into the zone of massive sulfides in the form of "injections" filling voids and cracks. In Fig. 2 (b), the silicate melt L_2 with a porphyritic structure fills the



a)



b)

Fig. 2. BSE images of the silicate part: a) Grt–Cpx matrix with intergranular glass (L_1); b) massive areas of injection glass (L_2) in the ore part.

The phase relations indicate the occurrence of several processes during the experiment. In the silicate part, partial melting of basalt took place at the P–T eclogite depth facies with the formation of Grt–Cpx restite with a small amount (< 1%) of intergranular silicate melt of ferrobasalt composition. The properties of Grt–Cpx restite, the value of the 2-sided contact angle between the crystals corresponded to the conditions of an open system, which contributed to the migration of the main volume of the melt through the intergranular space and its intrusion into the weakened zones of the ore part. During migration and intrusion, the melt captured individual portions of layered sulfide melts.

This study is fulfilled under Research program FMUF-2022-0001 of the Korzhinski Institute of Experimental Mineralogy, with the support of the Russian Science Foundation grant No 21-17-00119

References

1. Litvin Yu.A. Physico-chemical studies of the melting of the deep matter of the Earth. M.: Science. 1991. 312 C.
2. Gorbachev N.S. Fluid-magma interaction in sulfide-silicate systems // International Geology Review. 1990. V. 32. No. 8. P. 749-836

space between segregations of the sulfide and metal phases. In terms of composition, L_2 corresponds to moderately alkaline picobasalts, is characterized by lower concentrations of FeO (about 30 wt.%), TiO_2 (1.5 wt.%), alkalis ($Na_2O + K_2O$ 3–4 wt.%), higher contents of MgO (4–5 wt.%) and CaO (up to 9 wt.%) compared to L_1 .

Limanov E.V.¹, Butvina V.G.¹, Safonov O.G.¹, Van K.V.¹, Vorobei S.S.²
Experimental study of the reaction of K-richrichterite formation at 3 GPa and 1000°C.
 UDC: 552.13

¹D.S. Korzhinski Institute of Experimental Mineralogy Russian academy of science, Chernogolovka, Russia
²Vernadsky Institute of Geochemistry and Analytical Chemistry, RAS, Moscow, Russia limanov.ev@iem.ac.ru,

Abstract. High degrees of modal mantle metasomatism lead to the formation of K-richrichterite, which is stable over a wide range of temperatures and pressures. Its appearance is due to the reaction $8En + Di + [1/2K_2O + 1/2Na_2O + H_2O] = K-Rct + 2Fo$, which was studied experimentally in the presence of fluid K_2CO_3 - Na_2CO_3 - CO_2 - H_2O at a temperature of 1000°C and a pressure of 3 GPa, at different Na/K ratios. At Na/K = 50/50 and 70/30, amphibole is formed at $(K_2CO_3 + Na_2CO_3)/(H_2O + CO_2) = 30/70$. With an increase in the activity of alkaline components, decomposition of clinopyroxene occurs, as well as a shift in the composition of amphibole in the case of Na/K = 50/50 towards K-richrichterite, and in the case of Na/K = 70/30 towards sodium analogues. In the Na/K = 30/70 system, the appearance of amphibole turned out to be impossible only at $(K_2CO_3 + Na_2CO_3)/(H_2O + CO_2) = 20/80$ and 30/70. Its presence at lower and higher alkali contents may be due to the alternating effect of the activity of water and alkaline components on the stability of amphibole. It has been established that the formation of K-richrichterite

depends not only on the alkalinity of the fluid, but also on the ratio of the alkaline components themselves.

Keywords: mantle metasomatism; fluid; experiment; amphibole; K-richterite

Modal mantle metasomatism is a process of mantle peridotites alteration during their interaction with fluids of different composition and origin, which results in the generation of minerals not characteristic of primary peridotite paragenesis, such as phlogopite, amphibole, titanates, carbonates, sulfides, etc. (O'Reilly & Griffin, 2013). High degrees of metasomatism lead to the K-richterite formation, a low-alumina amphibole that is stable over a wide range of temperatures and pressures (Trønnes, 2002). Its generation occurs during the reaction $8\text{En} + \text{Di} + [1/2\text{K}_2\text{O} + 1/2\text{Na}_2\text{O} + \text{H}_2\text{O}] = \text{K-Rct} + 2\text{Fo}$, with the participation of water-carbon dioxide fluid and salt components. The ratio of alkaline components in amphibole depends on their ratio in the fluid (Zimmermann et al., 1997) and is a function of pressure (Konzett & Ulmer, 1999).

K-richterite formation was studied under conditions of the upper mantle (1000°C and 3 GPa) at various Na/K ratios. The research products are shown in Table 1. Similar patterns were noted in the I-Kr and II-Kr systems. The system contains an association of two pyroxenes and olivine at a relatively low content of alkaline components in the fluid (Fig. 1a). The formation of amphibole (Fig. 1b) turned out to be possible at $\text{Na}_2\text{CO}_3 + \text{K}_2\text{CO}_3 / \text{H}_2\text{O} + \text{CO}_2 = 30/70$. Its generation is accompanied by the formation of olivine, as well as clinopyroxene decomposition up to its complete disappearance and

preservation only as an inclusion in other phases. Changes in the component composition of minerals with an increase in fluid alkalinity turned out to be the following: in the I-Kr system, the clinopyroxene decomposition leads to an increase in calcium in orthopyroxene, and the amphibole composition shifts towards K-richterite; in the II-Kr system, the calcium content of both pyroxenes decreases (Fig. 2a), and the amphibole composition shifts towards the sodium series (Fig. 2b).

The high K/Na ratio in the III-Kr system leads to the possibility of amphibole formation even at the minimum salt content in the fluid. Its absence at ratios $\text{Na}_2\text{CO}_3 + \text{K}_2\text{CO}_3 / \text{H}_2\text{O} + \text{CO}_2 = 20$ and 30, and its presence at higher alkali activity may be due to the alternating effect of the activities of water and alkaline components on the formation of amphibole. Instead of amphibole, under these conditions, the system contains needles of an alkaline quenching phase (the length of the needles is up to 2 µm). High water activity stabilizes K-richterite in the III-Kr system. The high activity of alkalis, on the contrary, stabilizes more sodium analogues.

The most favorable conditions for the amphibole formation with a high potassium content were demonstrated by a system with a high K/Na ratio. The complicated formation of K-richterite in the experiment indirectly determines its rare occurrence in natural samples. The obtained effects are important for assessing the activity of alkaline components in the fluid, as well as the pressure in the processes of modal mantle metasomatism of upper mantle peridotites.

Table 1. Products of experiments carried out at 3 GPa and 1000°C

Na/K \ $\text{Na}_2\text{CO}_3 + \text{K}_2\text{CO}_3 / \text{H}_2\text{O} + \text{CO}_2$ mol.%	10	20	30	40	50	60
50/50 (I-Kr composition)	Ol	Ol	Ol	Ol	Ol	Ol
	-	-	Amp	Amp	Amp	Amp
	Di	Di	Di	Di	Di* B Ol	-
	Opx	Opx	Opx	Opx	Opx	Opx
70/30 (II-Kr composition)	-	Ol	Ol	Ol	Ol	Ol
	-	-	Amp	Amp	Amp	Amp
	Di	Di	Di	Di	Di	Di* in Ol
	Opx	Opx	Opx	Opx	Opx	Opx
30/70 (III-Kr composition)	Ol	Ol	Ol	Ol	Ol	Ol
	Amp	-	-	Amp	Amp	Amp
	Di	Di	Di	Di	Di	Di
	Opx	Opx	Opx	Opx	Opx	Opx

Note: * - phase in the form of an inclusion.

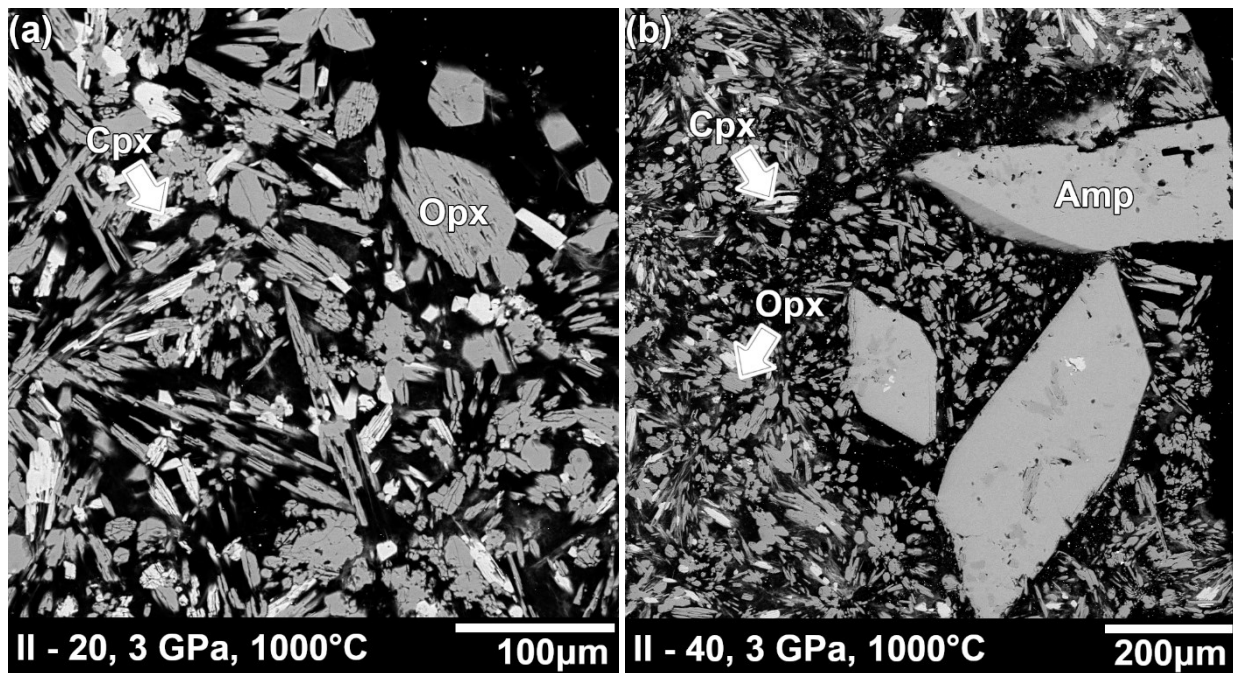


Fig. 1. Images of samples in reflected electrons: a) an association of two pyroxenes, in a sample where amphibole was not found; b) large amphibole crystals (up to 500 μm in length) surrounded by crystals of two pyroxenes. Dark inclusions inside the amphibole are orthopyroxene, light inclusions are clinopyroxene.

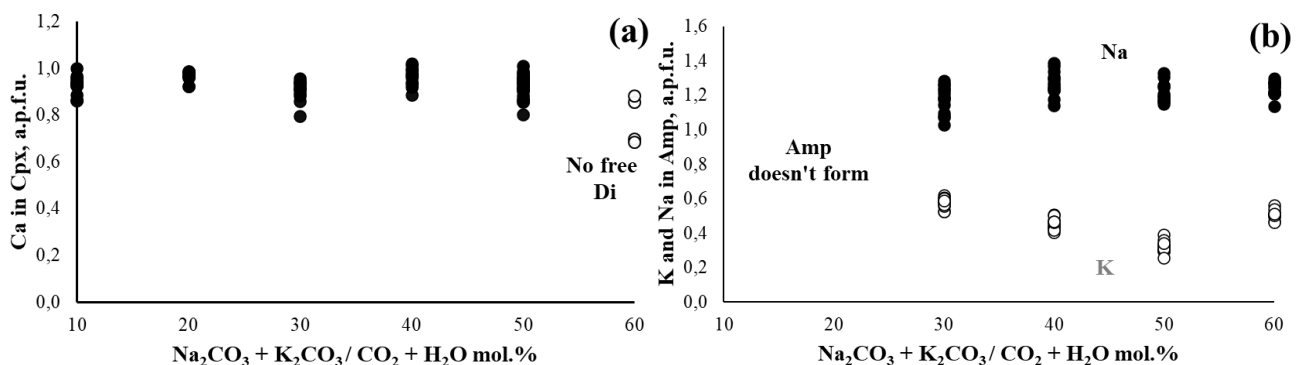


Fig. 2. a) Plot of the dependence of the change in the content of Ca apfu in clinopyroxene depending on the alkalinity of the fluid in the II-Kr system; b) change in the content of K and Na apfu in amphibole, depending on the composition of the fluid in the II-Kr system.

References

1. Konzett J., Ulmer P. The stability of hydrous potassic phases in lherzolitic mantle – an experimental study to 9.5 GPa in simplified and natural bulk compositions. // *Journal of Petrology*. — 1999. — V. 40, № 4. — P. 629-652.
2. O'Reilly S.Y., & Griffin W.L. *Metasomatism and the chemical transformation of rock*. // Springer: Berlin-Heidelberg, 2013. — P. 471-533.
3. Trønnes, R.G. Stability range and decomposition of potassic richterite and phlogopite end members at 5-15 GPa. // *Mineralogy and Petrology*. — 2002. — V. 74, №2-4. — P. 129-148.
4. Zimmermann R., Gottschalk M., Heinrich W., Franz G. Experimental Na-K distribution between amphiboles and aqueous chloride solutions, and a

mixing model along the richterite-K-richterite join. // *Contributions to Mineralogy and Petrology*. — 1997. — V. 126, № 3. — P. 252-264.

Sharapova N.Y.¹, Bobrov A.V.¹, Spivak A.V.²
Phase relations in the Fe-Ni-S system under the parameters of diamond formation. UDC: 550.4.02; 549.322; 543.42

¹Faculty of Geology, Lomonosov Moscow State University, Russia, Moscow, 119991 sharapovaninel@gmail.com archi3@yandex.ru ²D.S. Korzhinskii Institute of Experimental Mineralogy of Russian Academy of Sciences (IEM RAS), Chernogolovka, spivak@iem.ac.ru

Abstract. The Fe-Ni-S model system at high pressures and temperatures describes the composition of a

monosulfide solid solution, which is common for inclusions in diamonds and mantle xenoliths. The diamond-forming efficiency of sulfide melts with dissolved carbon has been demonstrated in some experimental series of papers. To determine phase relationships, a series of experiments was carried out at $P=7.0$ GPa and $T=900\text{--}1600^\circ\text{C}$ on a toroid-type anvil apparatus at IEM RAS. As a result, T-X phase diagram in FeS-NiS system was created. According to the findings a continuous series of solid solutions of sulfide minerals is formed in the studied range of compositions. Temperature-related evolution of monosulfide solid solution and sulfide melt composition under the conditions of diamond depth facies is traced.

Keywords: phase relations; sulfides; inclusions in diamond; high pressure and temperature

The Fe-Ni-S model system at high pressures and temperatures describes the composition of a monosulfide solid solution, which is common for inclusions in diamonds and mantle xenoliths. The diamond-forming efficiency of sulfide melts with dissolved carbon has been demonstrated in a number of experimental works (Litvin et al., 2002; Shushkanova et al., 2008; Palyanov et al., 2021, etc.). It has also been found that heating diamonds under pressure to a temperature higher than the melting point of sulfides does not change the position of sulfide inclusions (Chepurov et al., 2008). It may therefore be presumed that trapped sulfide inclusions remain stable in natural diamonds in the post-crystallization period during their residence in the mantle. Thus, the study of their behavior at high temperatures and pressures is directly related to the conditions and environment of diamond formation (Chepurov et al., 2008). In addition, the use of chemical composition of sulfide inclusions, along with the mineral association of silicates and oxides, makes it possible to identify P-peridotite and E-eclogitic types of diamond parageneses (Garanin, 2006).

To establish phase relations in this system a series of experiments was carried out at $P=7.0$ GPa and $T=900\text{--}1600^\circ\text{C}$ on a toroid-type anvil apparatus

at IEM RAS. The starting material is homogenized mixtures of different iron and nickel sulfides, which were previously synthesized at the Laboratory of Electrochemistry Thermodynamics and Physics of Minerals of IEM RAS. Solid-phase synthesis includes compounds and members of solid solutions (mol %) based on FeS-NiS with ratios: 10–90, 25–75, 50–50, 75–25, 90–10. During the experiment at 7.0 GPa, the melting temperature for NiS was about 900°C and for FeS it exceeded 1750°C (in this series of experiments it was not established to better identify value). The study of surface morphology identification of phase contrast and chemical heterogeneity was carried out by using scanning electron microscopy and the composition of resulting phases was refined by electron probe analysis.

According to identified morphological features and phase composition, the samples can be divided into three types. The first type is sulfides with isometric usually xenomorphic precipitates, in which the conditions of complete melting were reached. The samples are characterized by well hardening structures in the form of light stripes of sulfide melt and the presence of a large number of small rounded pores (Fig. 1, 2). The second type of samples represents homogeneous dense masses of isometric grains Mss (monosulfide solid solution), which composition is similar to the initial mixtures (Fig. 3). The third type fixes the conditions of partial melting. On the surface of the samples there are phenocrysts of Mss based on Fe or Ni immersed in a sulfide melt (Fig. 4).

If we consider phase relations, these sulfides are the most important, because compositions of Mss and the equilibrium sulfide melt naturally differ in them. The $[\text{Me}/\text{S}]$ ratio for a monosulfide solid solution is usually slightly less than 1 while for a melt $[\text{Me}/\text{S}] > 1$. This difference is best seen in the Fe-Ni-S diagram (Fig. 5).

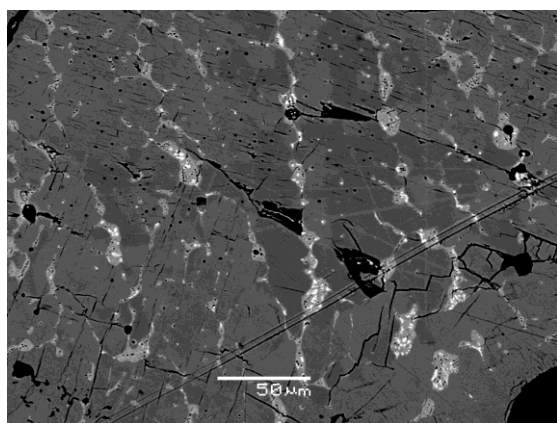


Fig. 1. Sample 930 NiS $T=1750^\circ\text{C}$

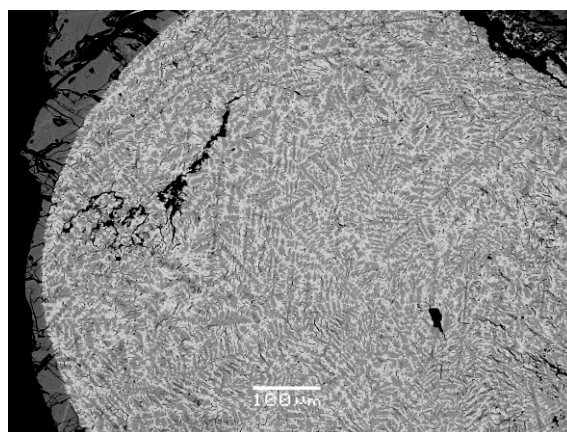


Fig. 2. Sample 936 $\text{Fe}_{0.25}\text{Ni}_{0.75}\text{S}$ $T=1300^\circ\text{C}$

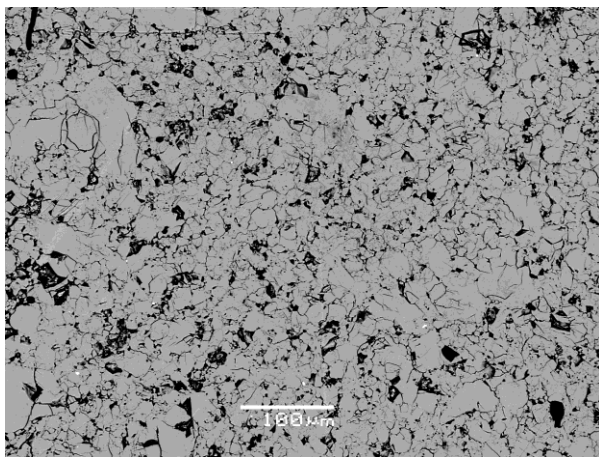


Fig. 3. Sample 947 $\text{Fe}_{0.5}\text{Ni}_{0.5}\text{S}$ $T=1000^\circ\text{C}$

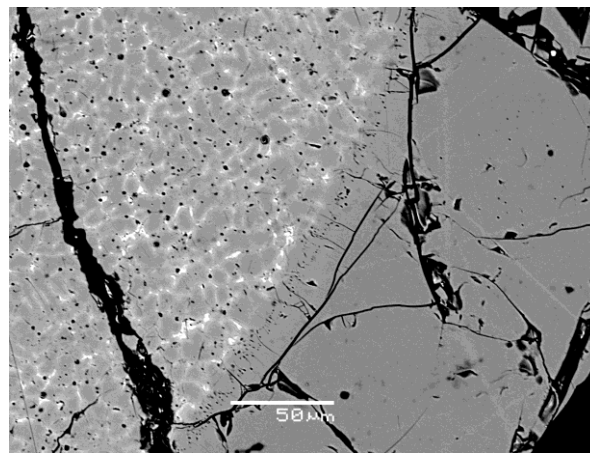


Fig. 4. Sample 950 $\text{Fe}_{0.75}\text{Ni}_{0.25}\text{S}$ $T=1500^\circ\text{C}$

According to morphological features, the conditions of complete melting (liquidus lines on the phase diagram), partial melting and solid-phase crystallization are quite well defined. Tie-lines have approximately the same slope, but differ in their length: temperature increase is accompanied by their shortening. In a series of experiments with the same

starting composition, temperature rise leads to an increase in nickel concentration in melts and coexisting Mss. Compared to the results of experiments that was carried out at atmospheric pressure (Kitakaze et al., 2011, 2016), we observe a narrowing of the space between the solidus and liquidus lines.

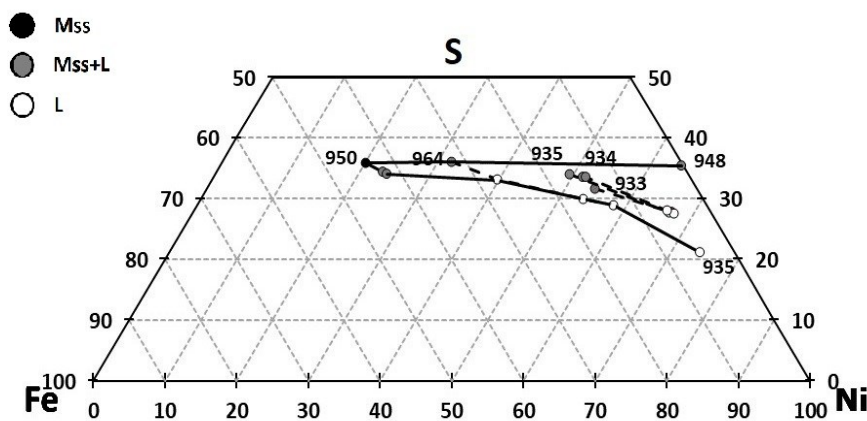


Fig. 5. Part of the phase diagram in the Fe-Ni-S system. The line marks the supposed boundary of the melt phase field. The dotted line shows tie-lines.

Comparing our data with composition of inclusions in natural diamonds, it can be noted that the resulting melt phases are characterized by a high content of nickel and an increase in the metals/sulfur proportion, while monosulfide solid solutions are enriched in iron. At the same time, analogy with natural systems is achieved only for starting compositions with $\text{Ni}/(\text{Ni}+\text{Fe})$ up to 0.75. The similarity of monosulfide solid solutions with both fields of sulfide inclusions in peridotite-type diamonds is also traced.

Homogeneous sulfides that differ in the initial component contents were selected for Raman spectroscopy. According to the results, the dependence of the position of the peaks on the

composition of sulfides has not been identified (Fig. 6).

The Raman spectra of monosulfide solid solutions are similar to nickel sulfide while the position and shape of the peaks for iron sulfide are different.

Structural analysis and literature data demonstrate that the unit cell parameters of solid solutions and nickel sulfide correlate with each other (Table 1). According to the literature data, troilite has a different space group and significantly differs in unit cell parameters.

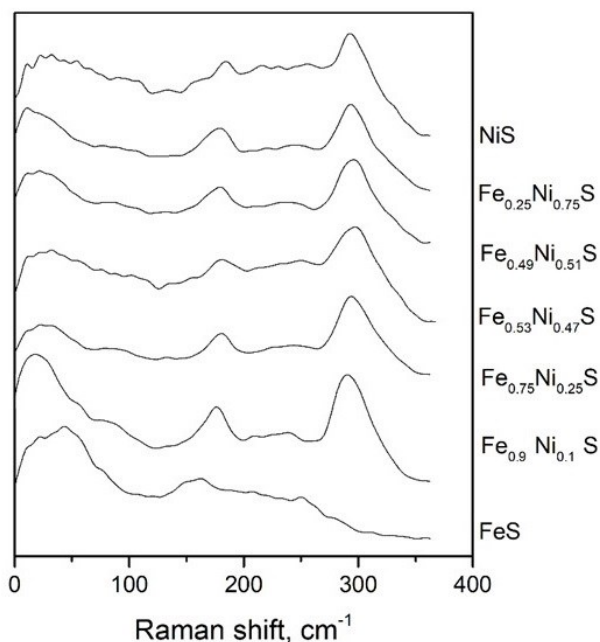


Fig. 6. Raman spectra of iron and nickel sulfides and solid solutions based on them.

Table 1. Structural data for members of solid solutions in FeS-NiS model system

Composition of sulfides	Space group	F.u.	a=b (Å)	c(Å)	V(Å ³)
FeS*	P $\bar{6}2c$	Z=12	5.9650(2)	11.7590(5)	362.34(2)
Fe _{0.9} Ni _{0.1} S	P 6 ₃ /mmc	Z = 2	3.449677	5.82544	60.03664
Fe _{0.5} Ni _{0.5} S	P 6 ₃ /mmc	Z = 2	3.449393	5.63286	58.04235
Fe _{0.25} Ni _{0.75} S	P 6 ₃ /mmc	Z = 2	3.451819	5.52916	57.05395
NiS	P 6 ₃ /mmc	Z = 2	3.441502	5.35568	54.93409

* Unit cell parameters for iron sulfide (Skála et al., 2006).

This study was carried out according to the research plan of the Laboratory of Earth's interiors, Faculty of Geology, Lomonosov Moscow State University.

References

- Garanin V. K. Mineralogy of kimberlites and related rocks of diamond-bearing provinces of Russia in connection with their genesis and prospecting. D.Sc. Thesis, MSU, 2006.
- Shushkanova A. V., Litvin Y. A. Diamond formation in sulfide pyrrhotite-carbon melts: Experiments at 6.0–7.1 GPa and application to natural conditions // *Geochemistry International*, 2008, T. 46. №. 1, 37-47.
- Litvin, Y. A., Butvina, V. G., Bobrov, A. V., & Zharikov, V. A. The first synthesis of diamond in sulfide-carbon systems: the role of sulfides in diamond genesis // *Doklady earth sciences*, 2002, 382, №. 1, 40-43.
- Chepurov A.I., Fedorov I.I., Sonin V.M., Logvinova A.M., Chepurov A.A. Thermal effect on sulfide inclusions in diamonds // *Russian Geology and Geophysics*, 2008. T. 49. №. 10, 738-742.
- Kitakaze A., Itoh H., Komatsu R. A revision of phase relations in the system Fe–Ni–S from 650 to 450°C // *Canadian Mineralogist*, 2011, 49, 1687–1710.
- Kitakaze A., Mzchida T., Komatsu R. Phase relations in the Fe-Ni-S system from 875 to 650°C // *Canadian Mineralogist*, 2016, 54, 1175–1186.
- Skála R., Císařová I., Drábek M. Inversion twinning in troilite // *American Mineralogist*, 2006. T. 91. №. 5-6, 917-921

Kuzyura A.V., Litvin Y.A., Spivak A.V. Influence of supercritical C-O-H-fluid on hyperbasic-basic evolution of magmatic and diamond-forming systems of the upper mantle. UDC: 552.11

Institute of Experimental Mineralogy Russian Academy of Sciences by D.S. Korzhinskiy, Russia, Moscow distr., Chernogolovka, Academician Osip'yan's street, 4, shushkanova@iem.ac.ru, litvin@iem.ac.ru

Abstract. The key mechanism of ultrabasic-basic evolution of magmatic and diamond-forming melts of the upper mantle is the peritectic reaction of olivine and jadeite-

containing melt with the formation of a garnet-containing association.

The influence of increased C-O-H-fluid contents on the possibility of the peritectic olivine reaction, its temperature, the compositions of reaction phases, and the starting point in mantle silicate-fluid magmatic olivine-jadeite-diopside – (5 wt. % C-O-H) and diamond-forming silicate - (Mg-Fe-Ca-Na-carbonate) - (7.5 wt. % C-O-N) systems was experimentally studied at 6.0 GPa and 700-1400°C. In the silicate-fluid system, the solidus and liquidus temperatures decrease, respectively, by 120 and ~60-80 °C compared to the dry silicate system. The olivine peritectic is shifted by ~10 wt. % towards olivine.

In the silicate-carbonate-fluid diamond-forming system, the olivine peritectic is still occurred at its temperature decreases by 280 °C, the solidus temperature by 380 °C in comparison with the silicate-fluid system. The CO₂ component carbonatizes silicates. The H₂O component is released into the gas-fluid phase on the solidus, creating a supercritical hydrothermal system that coexists with solid silicates and/or carbonates.

Keywords: C-O-H-fluid, ultrabasic-basic evolution, silicate-carbonate-fluid system, peritectic reactions, mantle metasomatizm, supercritical hydrothermal system

At the conditions of the upper mantle multi-component compositions of magmatic silicate-oxide and diamond-forming silicate-oxide-carbonate-carbon systems include fluid compounds. The study of fluid inclusions in diamonds provides unique information about the composition of volatile in parental medium of diamond crystallization (Navon et al., 2017). The findings of fluid inclusions in single-crystal diamonds correspond to composition to the components of C-O-H±N±S-fluid, such as CO₂ and H₂O (Jablon, Navon, 2016; Nimis et al., 2016). Water and carbon dioxide are the main volatile components in volcanic gases (Symonds et al., 1994). Liquid water and gas CO₂ are defined as independent phases in hermetic microinclusions in diamonds at room temperature (Schrauder, Navon, 1994; Izraeli et al., 2001). Probably, H₂O and CO₂ should be part of deep metasomatic fluid, which silicate rocks of the mantle are exposed to, according to the mantle-carbonatite theory (Litvin, 2017). Their interaction leads to formation of carbonate melts, which the host silicate rocks, as well as carbon, water, and carbon dioxide are dissolved in. This is how the chambers of parental diamond-forming carbonate-silicate melts are formed. The lifetime of such a chamber is limited by the time of fluid intake. A chamber gradually cools and crystallizes. Geochemical reactions occur in a chamber during process of fractional crystallization of diamond-forming carbonate-silicate melts. As a result, continuous series of diamond-bearing peridotite-pyroxenite-eclogite rocks are found in xenoliths.

Physicochemically, the possibility of a paragenetic peridotite-eclogite transition can be

realized as a result of fractional evolution of a substance of primitive garnet lherzolite of the upper mantle. The elimination of olivine and orthopyroxene can provide peritectic reactions, they lead to transformation of the original ultrabasic system Ol-Opx-Cpx-Grt into a bimineral eclogite system Cpx-Grt.

Peritectic reactions with elimination of olivine and orthopyroxene were experimentally demonstrated. The reaction of clinopyroxenization of natural orthopyroxene occurred in experiments at 4 GPa (Litvin, 1991), when the melting of the Ol-Opx-Cpx-Grt mantle system was investigated. The reaction interaction of forsterite and jadeite with the formation of garnet was experimentally detected at pressures above 4 GPa, at 6.5 GPa, at 7 GPa. It should be noted in magmatic and diamond-forming systems the reaction is possible when concentration of the jadeite component increases to a system-forming level only (Litvin et al., 2019).

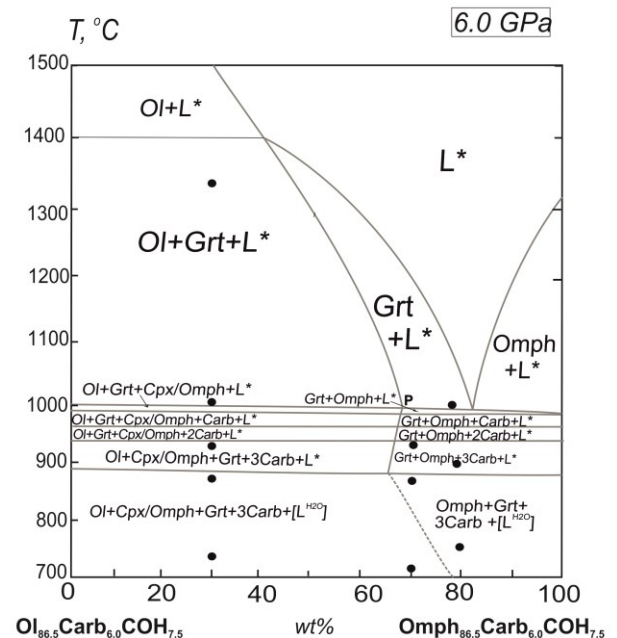


Fig.1. Phase diagram of the silicate-carbonate-fluid system Ol-Cpx-Jd-Carb-(C-O-H)-fluid in its polythermal section Ol_{86.5}Carb_{6.0}(C-O-H)_{7.5} – Omph_{86.5}Carb_{6.0}(C-O-H)_{7.5}

In the olivine-diopside-jadeite (Ol-Di-Jd) silicate system, the peritectic reaction of olivine granatization has been experimentally substantiated, a structure of the liquidus of the Ol-Di-Jd system has been determined, and its critical role as a "physico-chemical bridge" between ultrabasic olivine-containing peridotite-pyroxenite and basic silicate-saturated eclogite compositions of substance of the garnet-peridotite facies has been revealed. All olivine disappears at 1380-1420°C and its content is ~30 wt. %Ol (Litvin et al., 2019).

The purpose of this work is to demonstrate physicochemically the possibility of hyperbasic-basic

evolution of mantle substance, including diamond-bearing one, and to determine the influence of C-O-H-fluid on the process. To achieve this goal, it is necessary to experimentally investigate peritectic reactions sequentially in systems ranging from pure silicate to silicate-carbonate-fluid systems.

These problems can be solved using experiment combined with theoretical physical and geochemical methods for studying phase equilibria only.

Earlier the authors carried out experimental studies on the melting of ultrabasic-basic silicate-fluid system olivine-jadeite-diopside-garnet-(C-O-H-fluid) at 6 GPa with a fluid content of 5 wt % (Litvin, Kuzyura, 2021). The peritectic reaction of olivine retains its primary importance, (C-O-H)-fluid components do not make dramatic changes in phase relations. At the same time, there are quantitative topological changes of parameters of its liquidus structure – decreasing temperatures of the solidus and liquidus boundaries, respectively, by 120 and ~ 60-80 °C, as well as a shift in the composition of the peritectic reaction of olivine with increasing concentration of the olivine-containing component by ~ 10 wt. %.

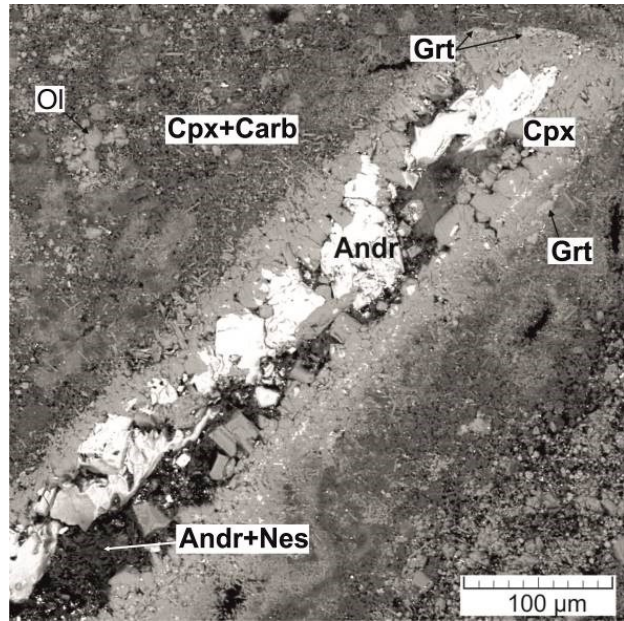


Fig. 2. «Geode» filled with liquidus phases (Grt, Cpx) and subsolidus carbonates. Sample 3291. Starting composition $-(\text{Ol}_{80.00}\text{Jd}_{12.40}\text{Di}_{7.60})_{80}\text{Carb}_{20}]_{92.5}\text{COH}_{7.5}$. 6 GPa. 1130 °C. Duration 95 min.

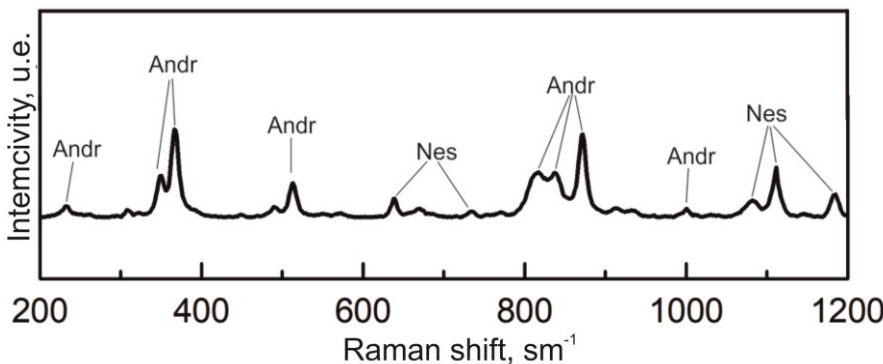


Fig. 3. Raman-spectrum of phases in «geode» - fine fusion of andradite (Andr) crystals with nesquegonite (Nes). Sample 3291

In this paper experimental studies of phase relations during melting of a model mantle diamond-forming carbonate-silicate-fluid system were carried out at pressure of 6 GPa and at temperature range of 700-1400 °C using a toroidal "anvil-with-hole" apparatus at the IEM RAS. Compositions of experimental systems were prepared from starting gel silicates and carbonates. The source of the fluid was oxalic acid dihydrate, which dissociated into CO₂, H₂O and H₂ during the experiments. The latter was most likely removed from the system due to its ability to diffuse through platinum. A crystal of synthetic garnet (andradite, Andr) was placed in a center of an ampoule to control the experimental conditions. Quenching samples were studied using scanning electron microscopy and microRaman spectroscopy analysis, Raman-spectroscopy was used to identify postsolidus phases. Based on the results of the experiments, a phase diagram of polythermal section $\text{Ol}_{86.5}\text{Carb}_{6.0}(\text{C-O-H})_{7.5}$ – $\text{Omph}_{86.5}\text{Carb}_{6.0}(\text{C-O-H})_{7.5}$ was plotted (Fig. 1).

Studies have shown the peritectic reaction of olivine persists in the silicate-carbonate-fluid system. Olivine, pyrope-almandine garnet, and omphacite are formed on the liquidus (Fig. 1, 2). The newly formed pyrope-almandine garnet of the pyrope-almandine series crystallized as a result of the peritectic reaction without the participation of seed andradite. Compared with the silicate-fluid system, the peritectic temperature decreases by 280, and the solidus temperature by 380 °C, and the composition of the peritectic reaction shifts with a decrease in the concentration of the olivine-containing component by ~ 10 wt. %.

The CO₂ component of the fluid contributes to partial carbonatization of silicates with formation of carbonate phases - calcite, magnesite, Na,Ca- and Mg,Fe-carbonates. These phases are fixed in samples at solidus and near-solidus temperatures.

At conditions of high-speed quenching (200 °C/sec) isolated cavities, as well as large enough hydrothermal structures of the geode type were formed in some samples. The cavities are filled with large silicate crystals (up to 120 microns) and a mixture of small carbonates and silicates in the intergranular space (Fig. 2). In one of these cavity aqueous carbonate nesquegonite $MgCO_3 \cdot 3H_2O$ was detected by Raman spectroscopy (Fig. 3). This indicates the presence of an aqueous solution during a formation of carbonate.

At experimental conditions carbon dioxide CO_2 and aqueous H_2O components are in the state of a fully miscible supercritical C-O-H liquid-fluid. The H_2O component is released into the gas-fluid phase on solidus, creating an independent supercritical hydrothermal system that co-exists in the open mode with subsolidus silicate and carbonate products of diamond-forming processes. At the same time, the supercritical H_2O fluid participates in the formation of independent chambers, as well as developed hydrothermal structures of the geode type.

Thus, the peritectic reaction of olivine retains its primary importance in the carbonate-silicate-fluid mantle system as (C–O–H)-fluid components do not make radical qualitative changes to phase relations during melting. The addition of fluid, however, leads to quantitative topological changes of the parameters of its liquidus structure. In addition, a "post-solidus" splitting into subsolidus mineral phases of the magmatic system and an open hydrothermal system coexisting with it in the subsolidus occurs with the participation of the C-O-H-fluid.

This study is fulfilled under Research program № FMUF-2022-0001 of the Korzhinski Institute of Experimental Mineralogy FMUF-2022-0001

References

- Green D.H., Falloon T.J., Taylor W.R. (1987) Mantle-derived magmas – role of variable source peridotite and variable C–H–O fluid compositions. In: *Magmatic Processes: Physicochemical Principles*. A volume in honor of Hatten S. Yoder, Jr. (Mysen B.O., Ed.). The Geochemical Society Special Publication No. 1. University Park: Pennsylvania, P. 139-154.
- Izraeli E.S., Harris J.H., Navon O. (2001) Brine inclusions in diamonds: a new upper mantle fluid. *Earth Planet. Sci Lett.*, 187, 323-332.
- Jablon B.M., Navon O. (2016) Most diamonds were created equal. *Earth Planet. Sci. Lett.* V. 443, P. 41-47.
- Litvin Yu.A. (2017) *Diamonds and Associated Phases*. Springer Mineralogy, 137 p.
- Navon O., Wirth R., Schmidt C. et al. Solid molecular nitrogen ($\delta-N_2$) inclusions in Juina diamonds:

- Exsolution at the base of the transition zone (2017) *Earth Planet. Sci. Lett.* V. 464, P. 237-247.
- Nimis P., Alvaro M., Nestola F. et al. (2016) First evidence of hydrous silicic fluid films around solid inclusions in gemquality diamonds. *Lithos.* V. 260. P.384–389.
- Schrauder M., Navon O. (1994) Hydrous and carbonatitic mantle fluids in fibrous diamonds from Jwaneng, Botswana. *Geochim. Cosmochim. Acta.* 58, 761-771.
- Symonds R.B., Rose W.I., Bluth G.J.S., Gerlach T.M. (1994) Volcanic gas studies: methods, results, and applications. In: *Volatiles in magmas* (Carroll M.R. and Holloway J.R., Eds.). Washington, DC: Mineral. Soc. Am. 30, 1-66.
- Litvin Yu. A. *Physicochemical studies of the melting of the deep-seated matter of the Earth*. Moscow: Science, 1991 (in Russian).
- Litvin Y. A., Kuzyura A. V. (2021) Peritectic reaction of olivine in the olivine–jadeite–diopside–garnet–(C-O-H) system at 6 gpa as the key mechanism of the magmatic evolution in the upper mantle. *Geochemistry International.* V. 59. 9. P. 813–839.
- Litvin Yu. A., Kuzyura A. V., Limanov E. V. The role of garnetization of olivine in the olivine–diopside–jadeite system in the ultramafic–mafic evolution of upper-mantle magmatism (experiment at 6 GPa) // *Geochemistry.* -2019. -V. 57. -P. 1045-1065.